MEASUREMENT OF WORK FUNCTION IN CF_4 GAS

by

IAN C. WOLFE

Submitted to the Department of Physics
in partial fulfillment of the requirements for the degree of

BACHELOR OF SCIENCE IN PHYSICS

at the

MASSACHUSETTS INSTITUTE OF TECHNOLOGY

June 2010

Author .....
Department of Physics
May 18, 2010

Certified by .....
Denis Dujmic
Research Scientist
Thesis Supervisor

Certified by .....
Peter Fisher
Professor
Thesis Supervisor

Accepted by .....
David E. Prichard
Senior Thesis Coordinator, Department of Physics

MEASUREMENT OF WORK FUNCTION IN CF_4 GAS

by

IAN C. WOLFE

Submitted to the Department of Physics
on May 18, 2010, in partial fulfillment of the
requirements for the degree of
BACHELOR OF SCIENCE IN PHYSICS

Abstract

CF_4 gas is useful in many applications, especially as a drift gas in particle detection chambers. In order to make accurate measurements of incident particles the properties of the drift gas must be well understood. An important property of CF_4 which is important for determining particle energy in detectors, the work function, is disputed and not well known. This thesis measures the work function of CF_4 gas for use in the Dark Matter Time Projection Chamber as well as all experiments that use CF_4 as a drift gas. This was accomplished by bombarding CF_4 in a drift chamber and ionizing it, then collecting the ionized electrons on an anode. The work function was found to be 33.8 ± 0.4 eV. This value was then crosschecked against P10, which is well understood.

Thesis Supervisor: Denis Dujmic
Title: Research Scientist

Thesis Supervisor: Peter Fisher
Title: Professor

Acknowledgments

First and foremost I would like to thank my advisor, Denis Dujmic. He set me up with this project and gave me invaluable help, direction, and guidance along the way; from help with UNIX and ROOT to particle physics theory. I would also like to thank Peter Fisher, the head of the DMTPC collaboration, for his oversight, his helpful advice on life and physics, and his piercing questions. I thank James Battat and Shawn Henderson of the DMTPC group for a very helpful discussion on ion mobility and long collection time in CF_4 gas. Finally, I would like to thank Regina Yopak and Emily Edwards for running Junior Lab while I was there and for being fun.

Contents

List of Figures

List of Tables

Chapter 1

Introduction

The purpose of this thesis is to measure the work function of CF_4 gas. The motivation for this measurement comes out of the Dark Matter Time Projection Chamber project at MIT, which uses CF_4 as a drift gas. The work function is critical for understanding DMTPC's results, particularly the energy of incident dark matter particles. This thesis makes an independent measurement of the work function, as there is some dispute over the value of this quantity in current literature. CF_4 has many qualities that make it a good candidate for a drift gas in general, so this thesis also provides a settlement of the value of the work function for future cases.

1.1 Search for Dark Matter

Based on astronomical observations, cosmology predicts that about 23% of the mass in the Universe is made up of dark matter. The evidence for such a theory is steadily building, and was originally put forward as a way to explain the movement of galaxies on the outer edges of galaxy clusters [1]. These galaxies rotate too rapidly for the visible mass of their parent cluster to hold on to them, and dark matter was invoked as a way to explain the difference between the observed and required galactic mass distributions [2]. Astronomical observations of luminous matter and of the Cosmic Microwave Background now provide a substantial base for dark matter theories [3].

A good candidate for dark matter is the Weakly Interacting Massive Particle

(WIMP). WIMPs are attractive potential dark matter particles because they have desirable theoretical properties both in cosmology and particle physics [3]. However, because these massive particles are so weakly interacting, they are very difficult to detect and have yet to be observed.

There are three general categories of WIMP detection: direct, indirect, and production is collisions of high energy proton beams (LHC). Indirect detection looks for WIMP annihilation products such as high-energy neutrinos or gamma rays. However, these products and their quantities are very dependent on the dark matter model that predicts them, and can be subject to variances in assumed parameters. While direct detection is still dependent on model parameters like density or velocity distribution of dark matter, it is the least model dependent by simply observing the nuclear recoils from WIMP collisions.

Directly discovering a WIMP will help validate a major theory in physics and also provide further insight into the nature of the universe by revealing the physical characteristics of the particle, such as its mass, spin, etc. Even a negative result helps to set limits on what characteristics a WIMP can have and assists in ruling out possible dark matter theories.

Direct dark matter detectors come in several general categories. Solid-state cryogenic detectors have large mass and a good signal-to-noise ratio. Liquid Xe, Ar, and Ne experiments are easily scalable up to large masses but generally have smaller signal production [3]. Gaseous experiments have the smallest detector mass, but are capable of reconstructing the direction vector of the WIMPs in addition to their energy, which is important for validating WIMP anisotropy, an important feature in many dark matter models [4].

1.1.1 DMTPC

The Dark Matter Time Projection Chamber (DMTPC) is a detector filled with tetraflouromethane (CF_4) gas under low pressure (75 Torr). When a WIMP strikes a ^{19}F atom within a CF_4 molecule, the massive dark particle causes a nuclear recoil of a few millimeters [5]. This recoil ionizes the particles along its trajectory (see

Section 1.2.2). The electrons produced by ionization inside the detector volume drift in a weak electric field toward a region with a high electric field where they cause electron cascades. These cascades multiply the number of electrons that finally cause scintillation to readable levels.

The photons emitted by scintillation are captured by a CCD camera and the drift electron charge is measured with charge-collection electronics. Nuclear recoil events leave easily distinguishable tracks across the view-field indicating incident direction in two dimensions. The z direction (directly into the camera) can be reconstructed by looking at track spreading along the drift direction. Energy is reconstructed from the light intensity of the track as well as the total charge collected on the anode.

The energy calculation of the DMTPC experiment is dependent upon how much energy it takes to ionize an electron from a molecule of CF_4. DMTPC uses its observed signals of light intensity and charge collected to determine the energy of a nuclear recoil, and thus the incident WIMP, as follows:

$$\begin{aligned} Y_{light} &= \frac{E_R Q_{fraction}}{W} \cdot G_{light} \cdot \varepsilon_{light} \\ Y_{charge} &= \frac{E_R Q_{fraction}}{W} \cdot G_{charge} \cdot \varepsilon_{charge} \end{aligned} \tag{1.1}$$

where Y_{light} and Y_{charge} are the total light and charge collected by the CCD and charge electronics, respectively. The first term gives the total number of primary-ionization electrons: E_R is the nuclear recoil energy, $Q_{fraction}$ is the fraction of the energy deposited into ionization, W is the average energy required to produce election-ion pair, also known as the work function (see Section 1.2). The second set of parameters are related to the amplification and detection of the signal: G_{light} is the average number of photons per primary-ionization electron, ε_{light} is the efficiency to detect a photon created in the amplification region. Similarly, G_{charge} is the total charge multiplication factor in the amplification region, ε_{charge} is conversion gain into voltage amplitude by the charge collection electronics.

The work function, W, for CF_4 has no agreed upon value, and so represents a potential error in the DMTPC's energy calculation, as shown in equation (1.1). The

goal of this thesis is the measurement of W, the ionization work function in CF_4 gas.

1.2 The Work Function

The work function of a gas is the average energy required to create one electron-ion pair. The work function also encompasses all the energy dissipated from an incident particle by secondary ionizations in addition to primary ionizations (see Section 1.2.2 for further discussion).

The formal definition for the work function, W is as follows [6]:

$$W = \frac{L}{\langle N_I \rangle} \left\langle \frac{dE}{dx} \right\rangle \tag{1.2}$$

Here, $\langle N_I \rangle$ is the average number of electrons created through ionization by an incident energetic particle. L is the length of the particle's flight path through the gas and $\left\langle \frac{dE}{dx} \right\rangle$ is the average energy loss per unit length along that path.

The value of W is found to vary with the energy of the incident particle, with less energetic particles requiring more energy to liberate one ion pair than more energetic particles. Above a certain threshold value W asymptotically approaches a single value. It is this value that is generally quoted as a gas' work function. The energy range of interest to dark matter detection is in the constant region of the work function.

1.2.1 W_α and W_β

It turns out that the nature of the high energy particle has a small effect on the value of the work function for that particle [6]. There is a difference of less than a few eV between the work functions for any particular gas or gas mixture when bombarded with either alpha or beta particles. For many gasses, such as H_2, the difference is 0.1 eV, while for gasses like C_2H_6 the difference is 2.2 eV. Hence, any measurement taken by either method is likely to fall within a few eV of each other. A plot of W values for several different gasses and mixtures, including the value obtained in this thesis,

can be found in Figure 5-1.

1.2.2 CF_4 Ionization and Dissociation

Ionization

In a typical ionization reaction the free CF_4 molecule interacts with an energetic particle. This fast particle donates some of its energy to the CF_4 molecule to put the CF_4 into an excited state. From this excited state, the CF_4 loses its electron and becomes CF_4^+:

$$CF_4 \rightarrow CF_4^* \rightarrow CF_4^+ + e^- \tag{1.3}$$

This is known as a primary ionization, and though it generally involves the liberation of one electron, can ionize two or more electrons simultaneously [6].

Most of the ions produced in the wake of an energetic particle like an alpha or a recoiling ^{19}F atom are not actually produced in primary ionizations. There are a series of mechanisms that cause secondary ionization reactions, the most common caused by electrons freed in the primary ionizations [6].

$$e^- + CF_4 \rightarrow e^- + CF_4^* \rightarrow e^- + CF_3^+ + e^- \tag{1.4}$$

In this secondary reaction, the electron interacts with a molecule of CF_4. The CF_4 is excited to CF_4^* before finally losing an electron in the final step. There are a number of other secondary ionization routes, such as through intermediate excited states that result in molecular combination freeing an electron [6].

Dissociation

At this point the free electron drifts away in the chamber's electric field, leaving the CF_4^+ molecule, which is unstable. The anion then follows one of two possible decay paths:

$$CF_4^+ \rightarrow CF_3 + F^+ \tag{1.5a}$$

$$CF_4^+ \rightarrow CF_3^+ + F \rightarrow CF_2^{2+} + 2F + e^- \tag{1.5b}$$

In the first decay path, show in equation 1.5a, the tetraflouromethane anion dissociates into a molecule of triflouromethane and a florine anion. This configuration is stable, and the F^+ will drift in the chamber's electric field, in the opposite direction of the electron freed up in equation 1.3.

The second decay path (equation 1.5b) first breaks into CF_3^+ and a free flourine molecule. CF_3^+ is also unstable and soon dissociates further to CF_2^{2+} and a second free flourine. This diflouromethane anion drifts in the chamber's electric field, eventually discharging on the chamber's cathode.

1.2.3 Review of Past Work

The work function W must be measured for every gas mixture. Most gasses and mixtures of gasses in common use in the field have very well measured work functions. The literature on CF_4 is not as cut and dried as most other gasses, despite CF_4's importance to high tech applications and its use as a drift chamber gas. The two papers that include W for CF_4 are Sharma (54 eV) [7] and Reinking et. all (34.3 eV) [8]. These two sources feature a significant discrepancy.

Sharma

Sharma's paper *Properties of some gas mixtures used in tracking detectors* lists a variety of useful properties and parameters for a number of gasses commonly used in particle detectors. The value for W_β listed for CF_4 is 54 eV [7]. This is the paper most often referenced when using CF_4 in time projection chamber and drift chamber experiments.

Reinking et. all

In *Studies of total ionization in gasses/mixtures of interest to pulsed power applications*, Reinking et. all conducted an extension of a previous study on the work function

and other properties of C_2F_6 and Ar/C_2F_6. The extended study focused on CF_4, mixtures of CF_4, and other perflourocarbons. The value for the work function, W_α of CF_4 found in the Reinking study is 34.3 eV [8]. This paper, focused towards pulsed power switching applications, is rarely used among the particle physics community.

1.2.4 Work Function Measurement Strategy

As the goal of this thesis is an independent determination of the work function, W, for CF_4 gas, the following section focuses on a derivation of the work function in terms of variables that are easily measured using a modified version of the DMTPC drift chamber.

To begin, I shall examine the section of equation (1.1) relating to the number of ionization electrons, N_{e^-} (this is also related to equation (A.4)):

$$N_{e^-} = \frac{E_R Q_{quench}}{W} \tag{1.6}$$

I assume that all energy of α particles goes into electron-ion pair production, so Q_{quench} is set to 1.

Q is the total amount of charge from the ionized electrons and is determined by:

$$Q = N_{e^-} \cdot Q_{e^-} \tag{1.7}$$

where $Q_{e^-} = 1.602 \cdot 10^{-19}$ Coulombs is the charge of a single electron, the elementary charge. Q can be related to the amplitude of a signal collected by charge-collection equipment:

$$Q = \frac{V}{g} \tag{1.8}$$

Here, V is the voltage of the signal, generally on a mV scale in this thesis, and g is the electronics gain in $\frac{V}{pC}$ which represents the total magnification of the electrons system from the preamplifier and amplifier.

Placing equations (1.7) and (1.8) into equation (1.6) and rearranging produces the

following:

$$W = \frac{gQ_{e^-}}{V} E_R \tag{1.9}$$

This is the equation used to determine the value of the work function, which for values of E_R large enough, is a constant.

Chapter 2

Experimental Set-Up

This project used a ^{241}Am alpha source to fire high (~5.5 MeV) energy alpha particles into a test chamber. These alphas ionize a large number of atoms as they pass through the CF_4 gas, creating an N_{e^-} somewhere on the order of 10^5. The large N_{e^-} created by these energetic particles also allows noise from the readout electronics to be ignored, making the final measurements more accurate. By running the chamber in ionization mode (no charge amplification) and collecting ionization electrons at the anode, I measured how many electrons had actually been created from the 5.5 MeV alpha particle. These measurements allowed me to arrive at the work function for the molecule. This in turn allowed a more accurate determination of G_{charge} for the DMTPC and all other experiments that use CF_4 gas.

2.1 Calibration

According to equation (1.9), the determination of W hinges on a measurement of V, the voltage of the signal collected by the electronics. It is V that would vary from gas to gas, all other variables being equal, and so in a sense I am actually measuring the V of CF_4.

Q_{e^-} is extremely well known, and the value $1.602 \cdot 10^{-19}$ Coulombs will be used throughout this thesis.

Before any measurement of V can be undertaken, the values of g and $E_{particle}$

must be determined for the particular electronics chain and radiation source used.

2.1.1 Electronics Calibration

From the collection anode, a short HV cable was run to a preamplifier. No voltage bias was applied during the calibration. From this point the signal was directed to a shaping amplifier on a low gain setting. The shaped output was then run to an oscilloscope, where the pulses were displayed and collected for processing.

The gain of this entire signal chain is g, as mentioned in section 1.2.4, and includes factors such as signal attenuation in the cables and the effects of the detector's capacitance in addition to the well known and selectable factors such as preamplifier and amplifier gain settings.

In addition, since the collection signal was expected to be small, the linearity of the preamplifier and amplifier were tested, as well as the noise signal of the entire chain.

Preamplifier

A Canberra Model 2006a Semiconductor Detector Preamplifier was used as the first step in the signal chain from detector to voltage output. This preamplifier has a decay time of 50 μs, which is much more than the expected collection time of CF_4 electrons (see Section 2.3). This means that the pre-amp will not lose charge during collection of electrons. It has a charge sensitivity (selected) of 47 $\frac{mV}{M\ ion\ pairs}$. Finally, of importance to the calibration discussion, it provides a test input jack with a capacitor of 3.3 pC/V [10].

To make accurate measurements it is important to verify the linearity of the gain for the readout electronics.

In addition to checking linearity, the testing examines the preamplifier for proper manipulation of the signal on its way to the next step in the signal chain. To simulate such a current pulse, an Ortec Model 419 Precision Pulse Generator creates a sharp negative spike followed by a long exponential decay back to zero voltage. The

preamplifier reverses the polarity of the pulse to positive.

In order to test the preamplifier's linearity, the preamplifier was attached to the pulse generator at the test jack from the attenuated output terminal. This pulse generator produces pulses between 0 and 1 V with noise $\leq 0.003\%$ of pulse amplitude [11]. This pulser was also attached via a t-connector to the Tekronix TDS 3014B oscilloscope to provide a base signal output. The preamplifier's output channel was then connected to the oscilloscope to provide a signal contrast. Finally, the preamplifier was powered by a Canberra Amp/TSCA 2015A, but not otherwise connected to it. View diagram 2-1.

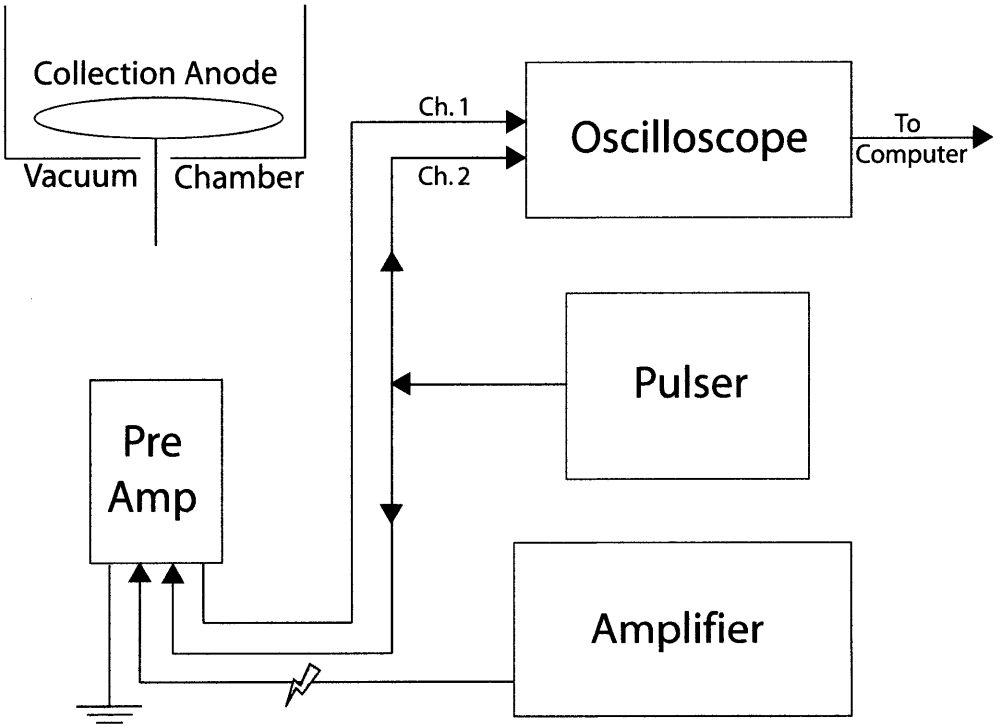

Figure 2-1: Preamplifier test schematic. Arrows indicate direction of signal. The yellow lightning bolt represents a power supply. Notice the pre-amp is not connected to the detector, nor does it send its signal to the amplifier.

A Root script was used to access the oscilloscope data remotely by computer and calculate the peak to peak and amplitude voltage of single runs triggered on the pulser

Pulser Parameter	Value
Normalize	1000
Pulse Height	858
Polarity	Neg
Ref Voltage	Int
Relay	Int Osc
Rise Time	Min
Attenuation	All Off

Table 2.1: Pulser Settings

signal. This enabled large numbers of runs to be conducted to improve statistics.

As expected, the preamplifier reverses the polarity of the signal and creates the proper pulse shape. There is a small dip in the preamplifier signal immediately following the main pulse, probably due to an impedance mismatch, however this effect is normal and does not affect the amplifier's interpretation of the signal.

The pulser voltage was varied from between 20 and 200mV in increments of 20mV over 100 trials, then passed to a standard linear fit in Root, shown in Figure 2-2. It was found that the preamplifier response was tightly clustered and submitted well to a linear fit (equation (2.1)). However, increasing voltages resulted in a slight spreading of the points away from the fit line.

$$\begin{aligned} Par0 = &\ 4.31 \cdot 10^{-4} \\ Par1 = &\ -0.434 \end{aligned} \tag{2.1}$$

As the error on the fit is negligible, a systematic error of %1 was assigned due to the fit procedure. This was estimated by looking at the spread of a cluster of points and comparing it to the mean value of the cluster.

There was one data point in each cluster of the dataset that was an outlier at a higher voltage. This is most likely some kind of systemic software error and not believed to be a function of the oscilloscope. These points were removed from the fit analysis.

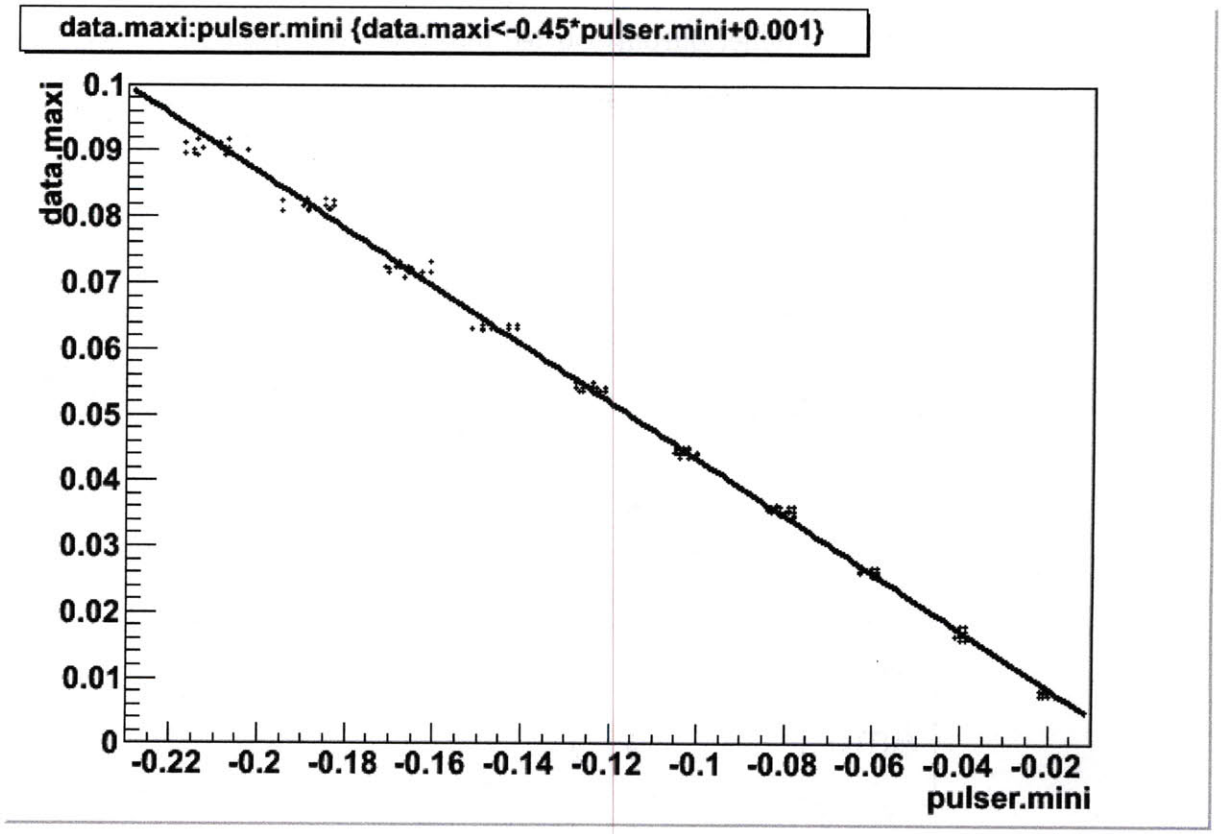

Figure 2-2: Preamplifier linearity plot, preamp signal vs. pulser signal, in volts. The measured voltages are tightly clustered around the fit line, with the exception of single outliers at each voltage measured. The fit variables are shown in equation (2.1), where par0 is the constant term and par1 is the linear term.

Amplifier

The testing set up for the amplifier was very similar to that used for the preamplifier with simply another link added to the signal chain. The pulser was connected to the preamplifier and directly to the oscilloscope, as before. The output signal of the preamplifier, which was powered as usual through the amplifier, was then fed into the amplifier input. The amplifier gain was then varied throughout testing as was the input voltage. The amplifier output was fed into the oscilloscope for comparison against the pulser signal. The amplifier signal chain test schematic is shown in Figure 2-3.

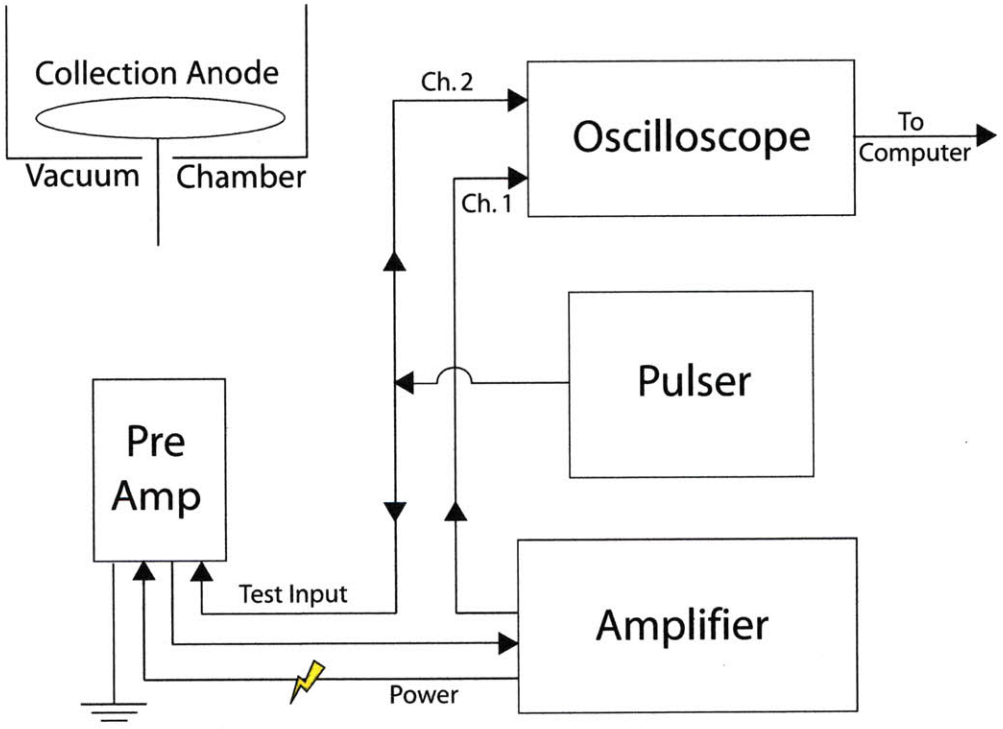

Figure 2-3: Amplifier test schematic. Arrows indicate direction of signal. The yellow lightning bolt represents a power supply. The signal chain is again run through the pre-amp's test input, not from detector input. The pre-amp is connected to the amplifier, which then connects to the oscilloscope.

As expected, the amplifier recognizes the pulser's signal, as converted by the

Pulser Parameter	Value	Amplifier Parameter	Value
Normalize	1000	Input:	+
Pulse Height	858	Window (ΔE):	1000
Polarity	Neg	Lower Level (E):	0
Ref Voltage	Int		
Relay	Int Osc		
Rise Time	Min		
Attenuation	All Off		

Table 2.2: Pulser and Amplifier Parameters for amplifier signal chain test.

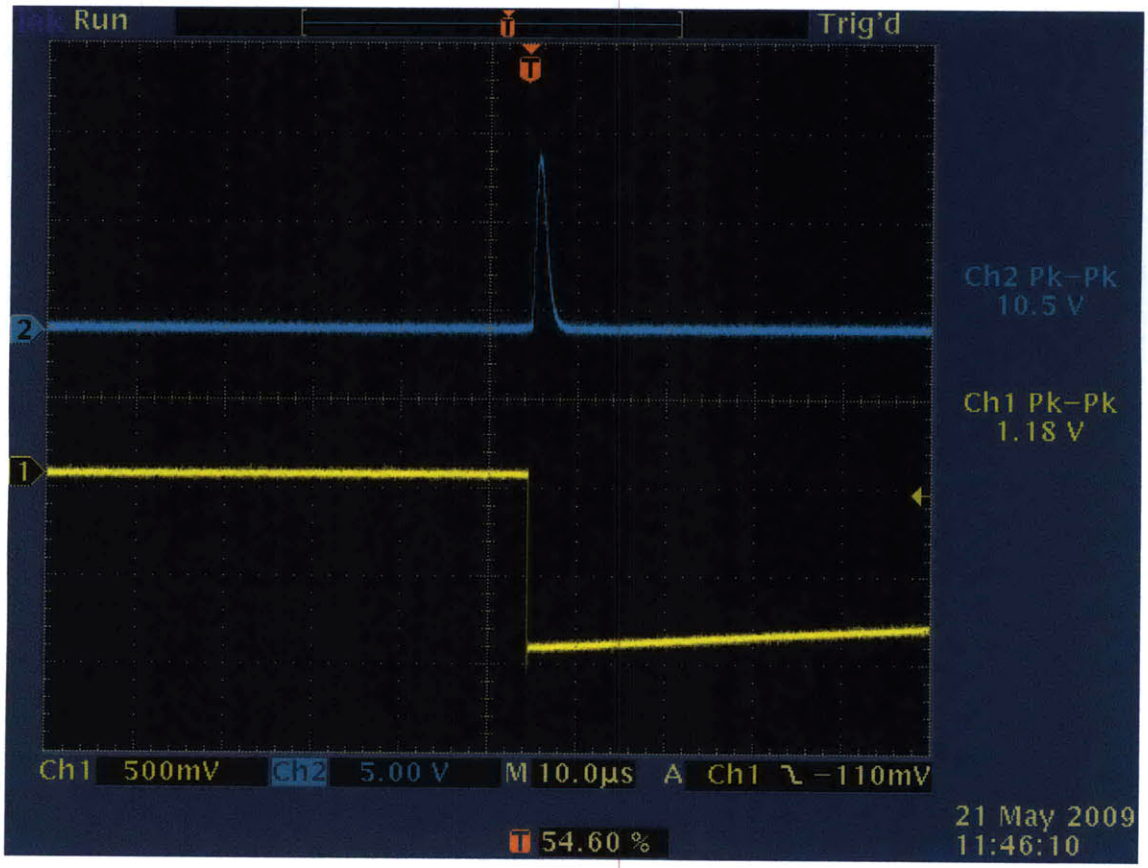

Figure 2-4: The amplifier signal as compared to the raw pulser signal. The pulse exhibits proper near-gaussian pulse shape and has been magnified by ~10 times in this screen capture, corresponding to an amplifier gain setting of about 8.

preamplifier. Figure 2-4 shows the amplifier's signal imposed on the pulser's output. The signal shows proper near-gaussian shaping and polarity.

The input voltage was varied between 10 and 150 mV in 10 mV increments over 150 trials over multiple gain settings. The data set was then interpreted by Root and submitted to a linear fit. The linear fit for one gain setting is shown in Figure 2-5.

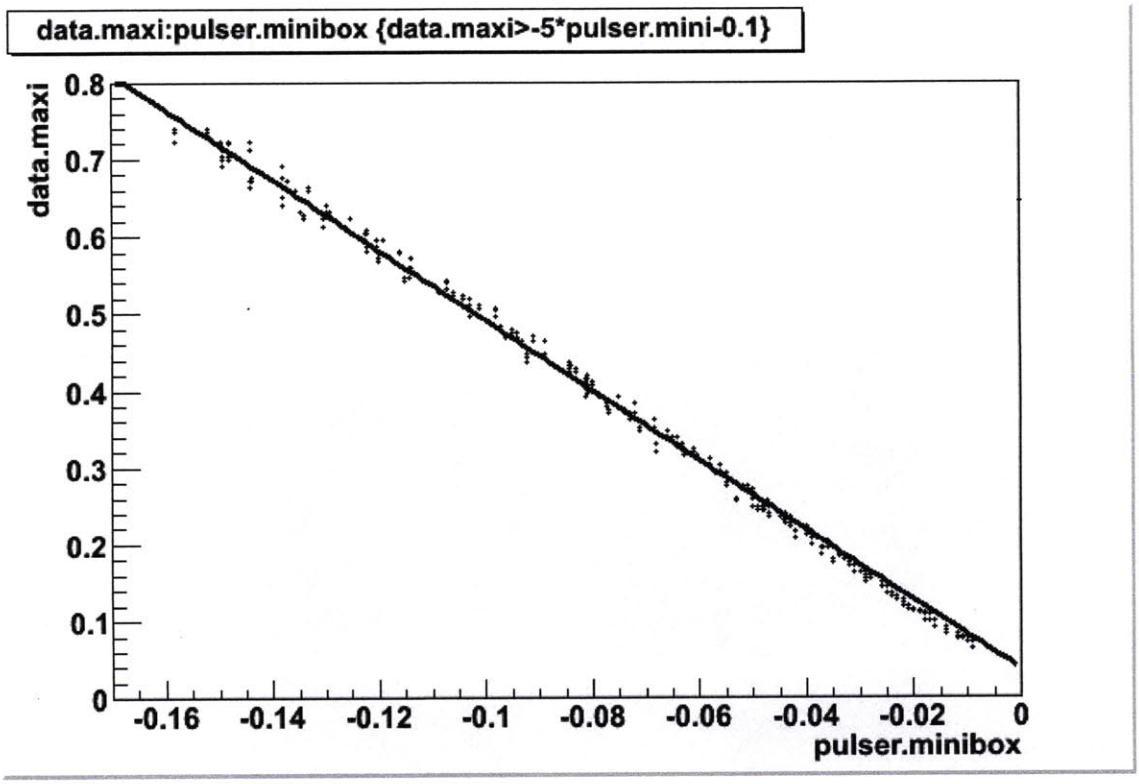

Figure 2-5: The linear fit of the amplifier signal chain data. The input voltage on this run was varied continuously over the range of 10-150 mV. The parameters of the fit show a slope of -4.54, which is consistent with the amplifier gain setting of 4.

The slope in Figure 2-5 is negative because the pulser outputs negative pulses. Thus, a negative slope indicates proper pulse polarity switching, which occurs at the preamplifier (see Section 2.1.1).

2.1.2 Gain Calibration

The capacitance of the detector has an effect on the gain of the electronic signal. The effect on the output signal can be examined by measuring the gain, obviating the need to measure the detector's capacitance by itself. This is also useful in that it

covers all capacitance contributions to the whole system including the detector, cable lengths, impurities, etc. This practice ensures the gain being measured is the gain of the entire electronics system in order to make the final prediction as accurate as possible.

The system gain was measured as in Section 2.1.1; by attaching the Ortec Model 419 Precision Pulse Generator to the preamplifier's Test Input connection and running a series of pulses of various heights through the system. In addition, the preamplifier was connected to the detector, to add the detector's capacitance to the system. The Root script was run for 1500 pulses. The pulse height was manually varied between about 5 and 40 mV in 5 mV steps. Each step collected between 200-250 points to measure the statistical spreading at any one voltage point.

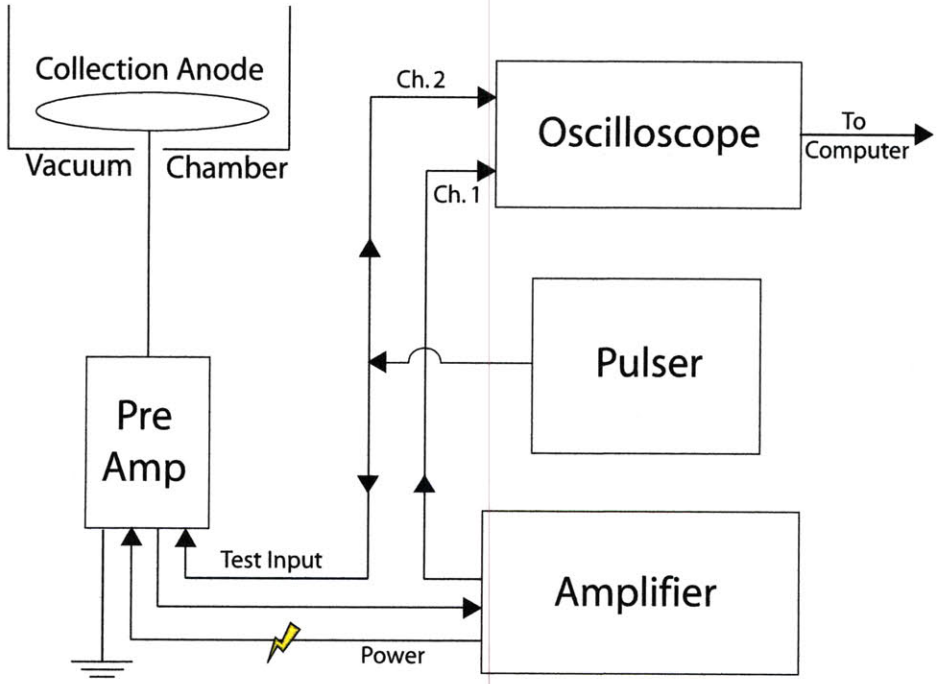

Figure 2-6: Gain testing schematic, including added capacitance from the detector.

The Work Function is determined by equation (1.9).

The gain, g, is determined by the equation:

$$g = \frac{Slope\ of\ Fit}{C_{in}} \tag{2.2}$$

Here, C_{in} is the input capacitance of the pre-amp's Test Input connection. For a Canberra 2006a Preamplifier, this test capacitor is 3.3 pF.

The data points collected with the Root script were then compiled and plotted, and a simple linear fitting script was run, as shown in Figure 2-7. The fit was determined

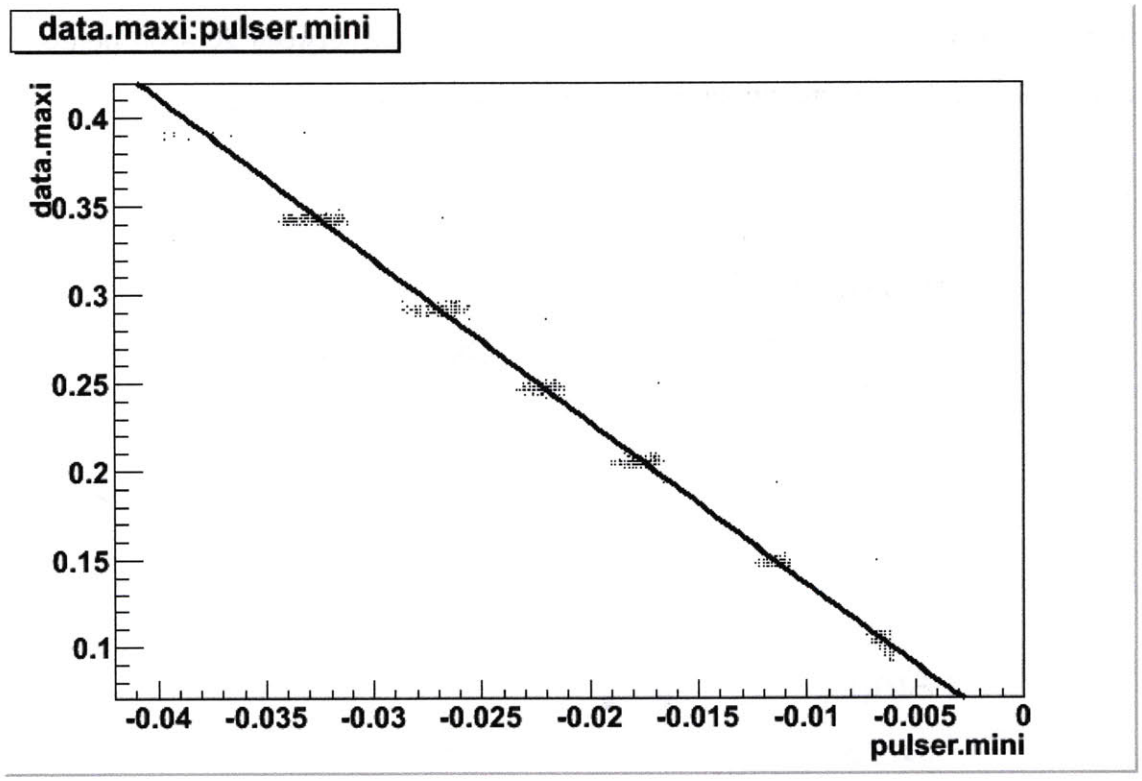

Figure 2-7: Plot of pulser voltage vs. amplifier voltage. Differences in detector capacitance are expressed by changes in the slope of this fit. The slope is negative because the pulser outputs negative pulses.

to be -9.230x + 0.042 V. The slope is negative because the pulser is actually pushing negative pulses, as explained in Section 2.1.1. Thus, a larger pulse height actually corresponds to a more negative pulse value as recorded by the oscilloscope and Root. The fit error of the slope was ±0.003 V. Placing the slope of the fit, 9.230, into

equation 2.2 gives the value of g.

$$g = 2.80 \pm 0.003\ (stat) \pm 0.01\ (syst)\ V/pC \tag{2.3}$$

The statistical error comes from the error on the fit, while the systematic error is derived from the difference of the fit's y-intercept from the origin as well as accounting for possible differences in the test input capacitor from 3.3 pC.

2.1.3 Alpha Source Calibration

The next calibration of importance is the energy of the fast particles used to cause ionizations. This experiment used an ^{241}Am alpha source. The theoretical value of ^{241}Am alpha emissions is around 5.5 MeV. However, the alphas must traverse a gold window of unknown thickness before reaching the chamber. The energy of the emitted alphas is important to finding W, as according to equation 1.9.

The detector used was a Canberra 450-20AM surface barrier detector, placed inside a small chamber formed by a cross-piping connection. The detector itself was placed in one arm of the cross, while the ^{238}U calibration source was placed in one of the arms offset by 90 degrees. This prevented the detector from reading direct decays from the uranium ore, and limited most alphas to a limited number of decay daughters of radon gas, as can be seen in Figure 2-8.

The uranium decay chain is shown in Figure 2-9. Those decay products that emitted alphas that were picked up by the detector are shown in red. The daughters that were seen in the detector and their decay energies are shown in Table 2.3. In

Element	E_{Qvalue} (MeV)	E_{Recoil} (MeV)	E_{Alpha} (MeV)
^{222}Rn	5.590	0.09	5.5
^{218}Po	6.115	0.12	6.0
^{214}Po	7.833	0.13	7.7

Table 2.3: Radon and its alpha emitting daughters that were detected in the alpha calibration set up. This table displays the total Q energy, the energy of the nuclear recoil, and the energy of the alpha itself.

order to get a significant peak, and to allow radon and its decay products to build in

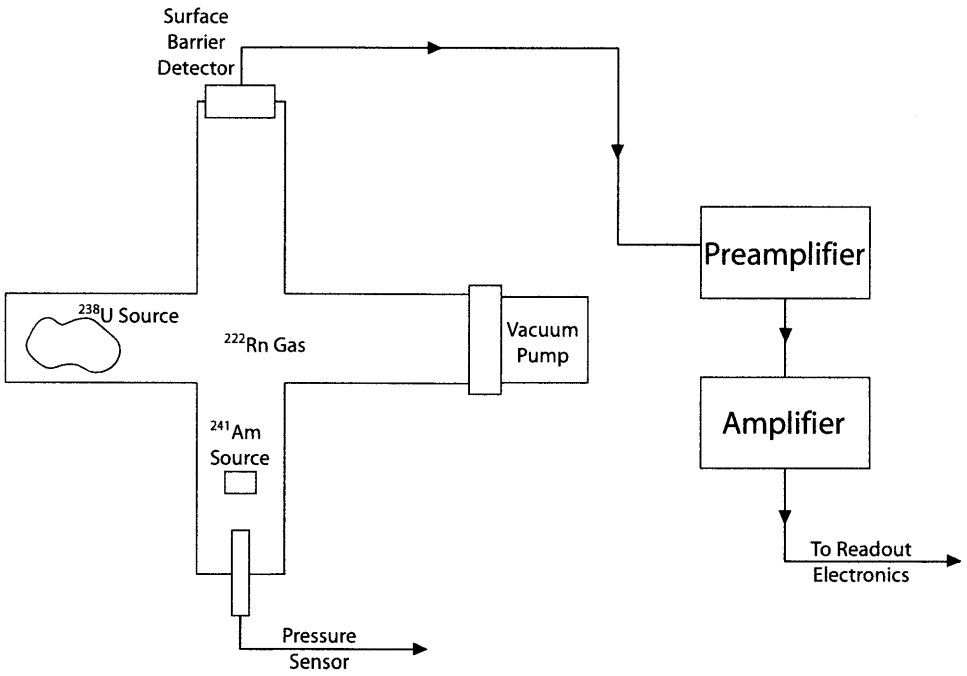

Figure 2-8: The test set up for the alpha calibration. The uranium source was placed in piping 90 degrees offset from the detector so that only radon decays would be visible to the readout electronics.

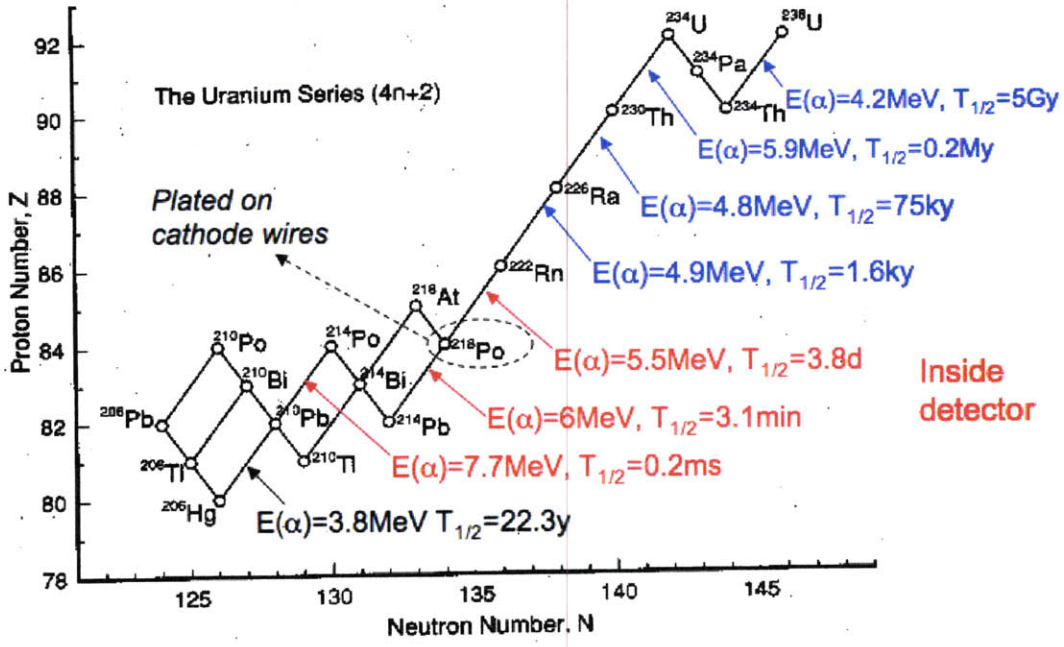

Figure 2-9: The ^{238}U decay chain. The daughters present to the detector were everything following ^{222}Rn, with the three shown in red as identifiable peaks.

the test chamber, the chamber was sealed and brought down to approximately 1e-3 Torr and left to run overnight. The data acquired is shown in Figure 2-10.

As can been seen, there are three main peaks, as well as a smaller one. This small peak is actually two peaks that are very close to each other. The three main peaks are due to radon-222 and its daughters. The two smaller peaks are products of the Thorium decay chain.

The uranium ore was then removed and the ^{241}Am alpha source was placed in the chamber, directly pointed at the detector. Data was collected over 5 seconds and the observed peak is seen in Figure 2-11.

The peak from the ^{241}Am source is actually three separate peaks. The main peak (86%) lies at 5.486 MeV. The second peak (12.7%) lies at 5.443 MeV, while the smallest peak (1.4%) is barely present at 5.391 MeV down at the trailing end of the peak. The fit used to find the peak position was a simple gaussian fit, with the mean of the gaussian taken to be the weighted average of the three peaks. The error in the fitting method was accounted for in the systematic error by finding the difference

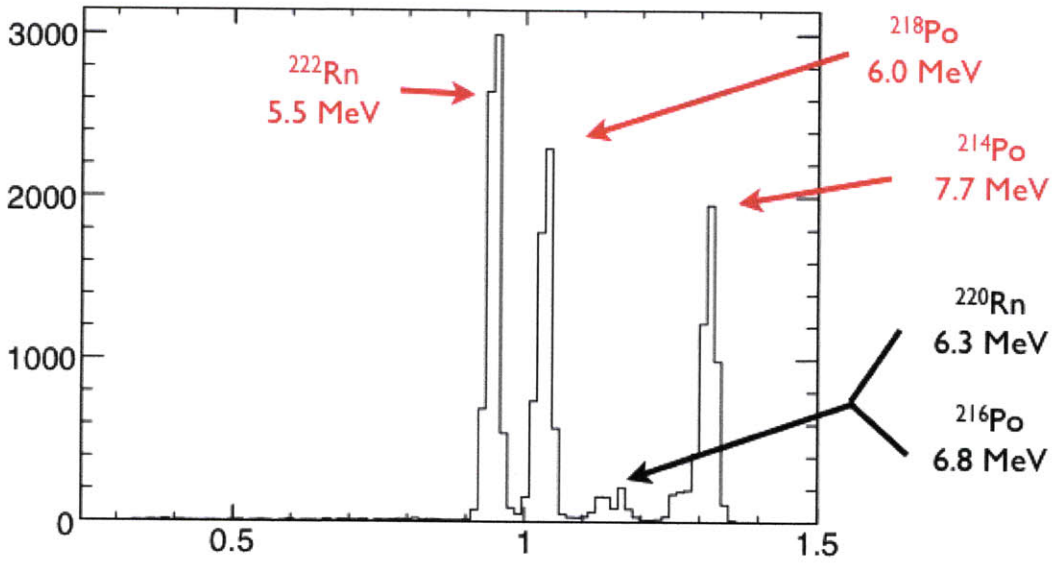

Figure 2-10: Data taken with the alpha calibration detector. Uranium ore was placed in the chamber and radon allowed to accumulate. The identified peaks are shown with red arrows and correspond to the red decay daughters of Figure 2-9 and the elements of Tables 2.3 and 2.4.

Element	Mean (V)	Error of Mean (V)	σ (V)
^{222}Rn	0.945	0.0001	0.011
^{218}Po	1.033	0.0001	0.013
^{214}Po	1.310	0.0003	0.020

Table 2.4: The detected daughters of the Uranium 238 decay chain. This table shows the mean voltage values induced by the detector for each peak, as well as the error on that mean and the spread of the peak.

between the 86% peak and the weighted average peak.

This method put the peak of the alpha source at 0.769 V in the detector output. The energy at this value could then be calculated by plotting the three known peaks and making a linear fit, then extrapolating this fit out to the proper value. The various known peaks are tabulated in Table 2.4. These points and associated errors were then plotted in Figure 2-12 and a linear fit was run. The output of the fit was of the form $y = ax + b$, with the value a fit at 6.029 $\pm$ 0.004 MeV V^{-1} and b found at -0.209 $\pm$ 0.004 MeV. Extrapolated to the alpha source's peak position at 0.769 V,

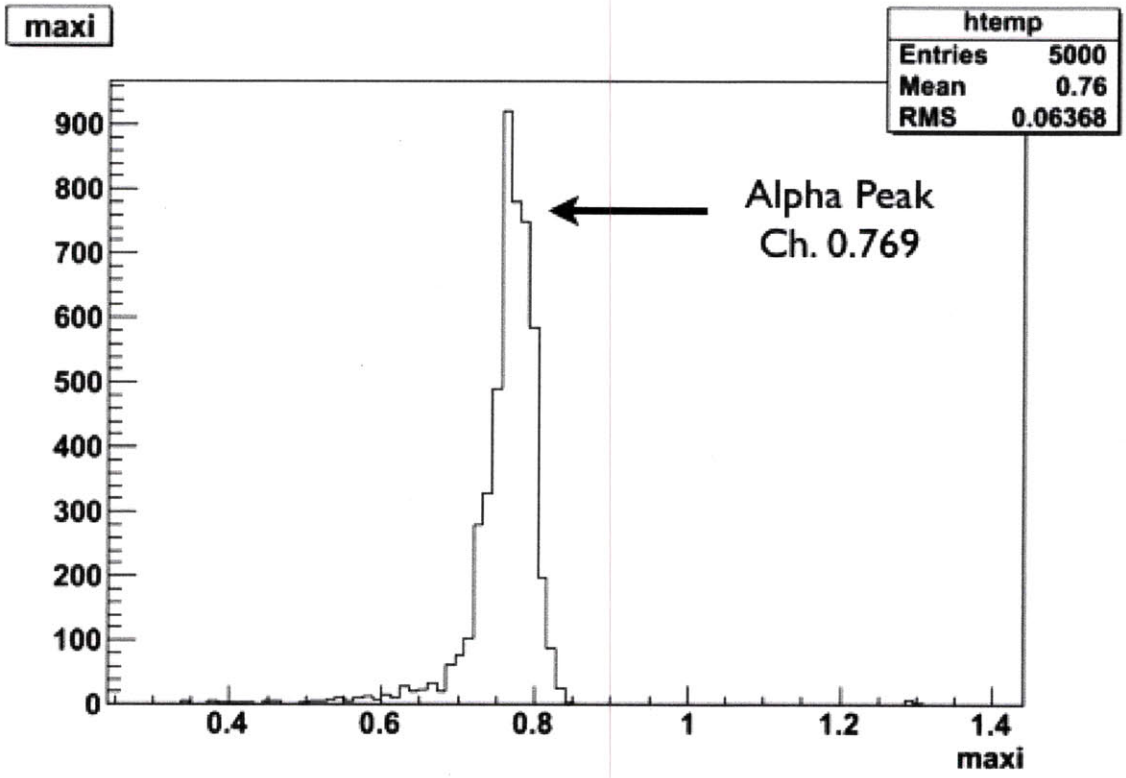

Figure 2-11: Data taken using alpha calibration detector where alpha source was pointed directly at detector. Data was collected over 5 seconds. The visible peak is actually composed of three separate peaks at 86%, 12.7%, and 1.4% of total alpha emissions. The peak was fitted as a single gaussian with a mean of 0.769 V.

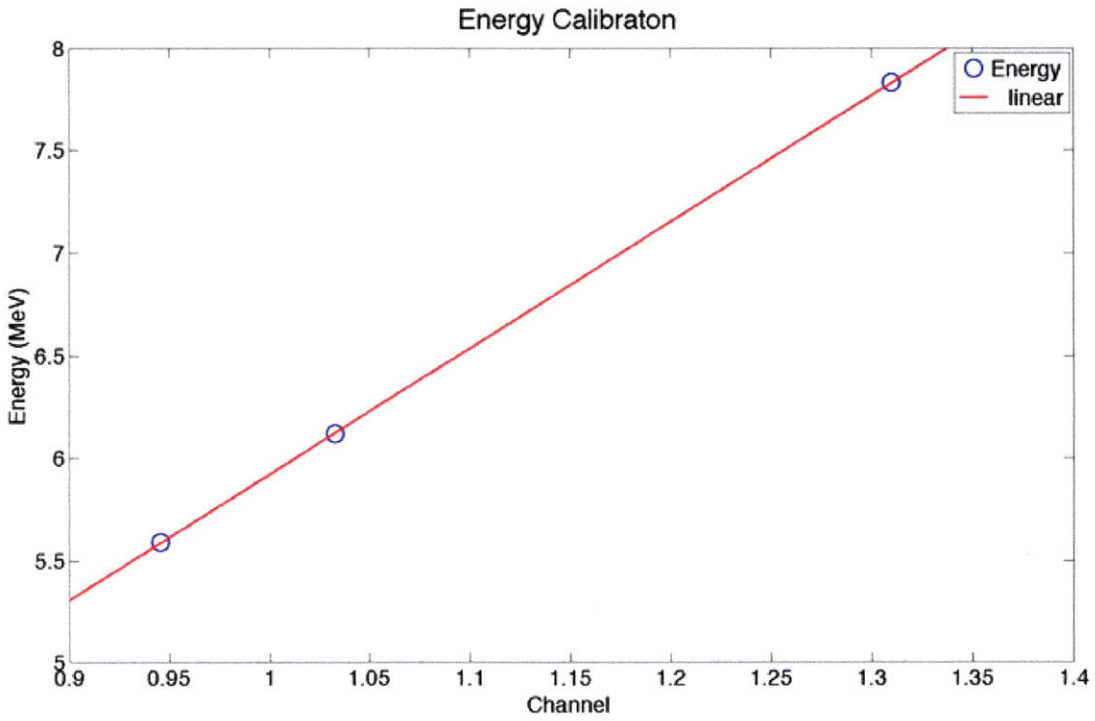

Figure 2-12: The alpha energies vs. detector voltage and associated errors for the decay daughters tabulated in Table 2.4. The energy of the calibration source was then extrapolated from the linear fit of these points.

an energy for the alpha source is arrived at:

$$E_\alpha = 4.282 \pm 0.005\ (stat) \pm 0.01\ (syst)\ MeV \tag{2.4}$$

The statistical component of the error is derived from the error on the fitting parameter a, the slope propagated out to the extrapolated distance. The systematic portion of the error derives from the fact that the slope of the fit does not perfectly intersect the origin, and instead passes just underneath it.

To reduce the alpha energy from 5.486 MeV to 4.282 MeV, SRIM [5] estimates an alpha must traverse about 2.8μm of gold foil.

2.2 Dual-Plate Ionization Chamber

It was found that running the DMTPC chamber in ionization mode was not sufficient for proper collection of ionization electrons because of mesh effects (see Appendix A.1).

A simpler dual-plate chamber was proposed as a solution to mesh transparency. This new chamber was simply two parallel copper plates spaced a distance of 2.8 cm apart from each other. The cathode was connected to the high voltage power system, while the anode was connected to the readout electronics and biased to ground. The ^{231}Am alpha source was fixed mid-way between the two plates, as shown in Figure 2-13(a).

As voltage was applied to the cathode, electrons ionized from the flight path of the alpha particles drifted down in an electric field and were collected on the anode plate. From here they were processed through a Canberra 2006a Preamplifier, and a Canberra Amp/TSCA 2015A Amplifier. This signal was then displayed on the Tekronix TDS 3014B Oscilloscope and digitally collected via network connection by a Root script.

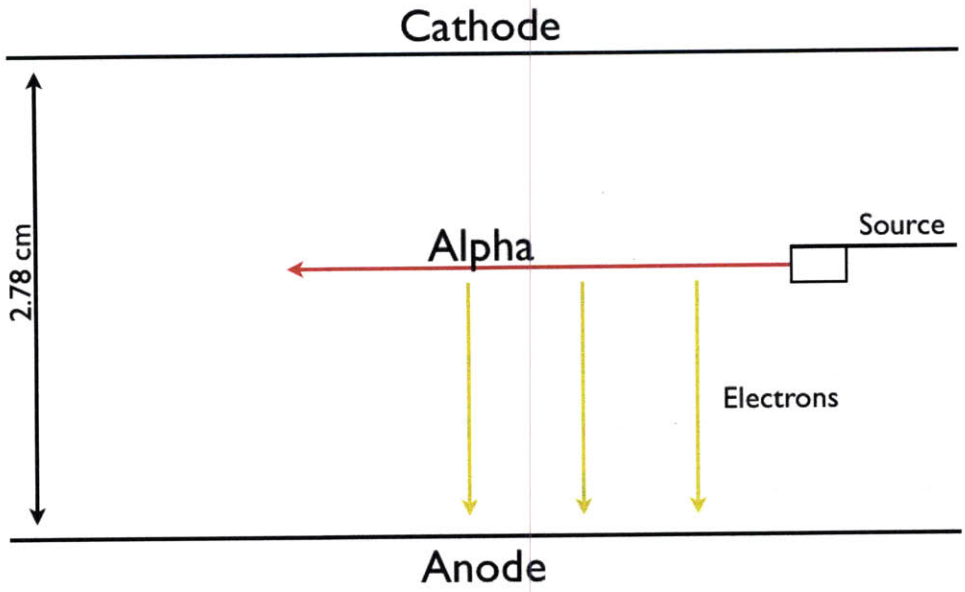

(a) Set-up Diagram

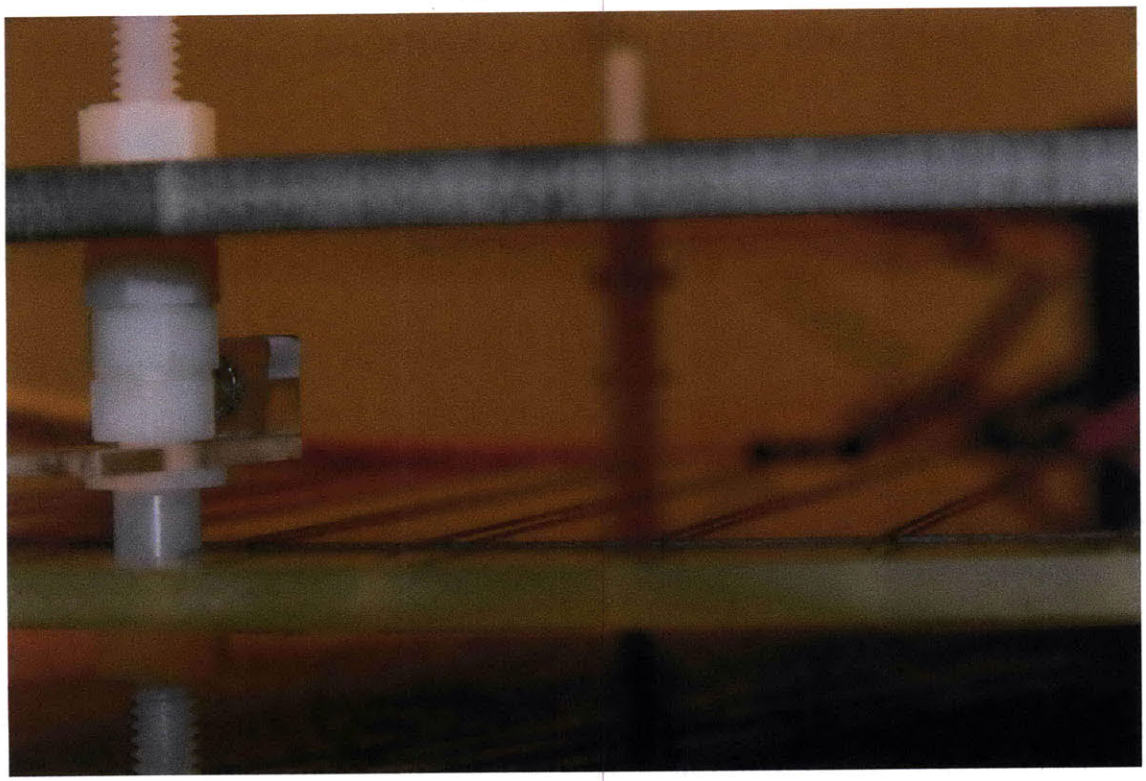

(b) Actual set-up

Figure 2-13: Simple schematic of the dual-plate experiment set-up. Two parallel copper plates were placed 2.78 cm apart, and the collimated alpha source placed midway between the plates. Ionized electrons then drift in the electric field applied between the two plates and are collected on the anode.

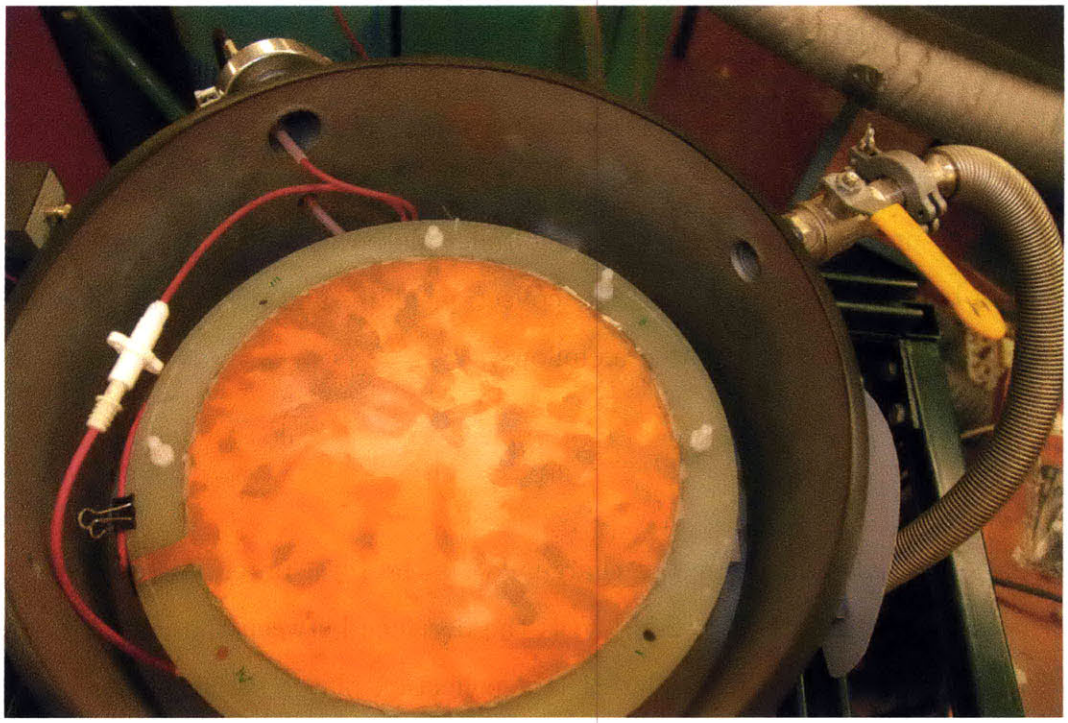

(a) Chamber open; top view

(b) Chamber Set-up

Figure 2-14: Photos of the actual chamber. Figure 2-14(a) shows the chamber opened from the top. The top copper plate can be seen inside, connected to the power source with the red cables. The large hose is attached to the turbo pump. Figure 2-14(b) shows the CF_4 tank and valves as well as the pressure readouts (showing 75.3 torr) in the foreground with the chamber in the background.

2.3 Signal in Ionization Chambers

With all other parameters calibrated, the measurement of V entirely determines the value the work function, W.

The voltage produced by a charge in a parallel plate detector is proportional to the distance between the charge and the collection plate, and also to the distance between the plates [3]. This is stated as follows:

$$P(y) = P_{12}\left(\frac{h-y}{h}\right) \tag{2.5}$$

$P(y)$ is the potential induced by the charge, P_{12} is the total potential between the plates (named 1 and 2 in Figure 2-15), h is the distance between the plates, and y is the distance of the charge from plate 1 (the collection plate). What this means is

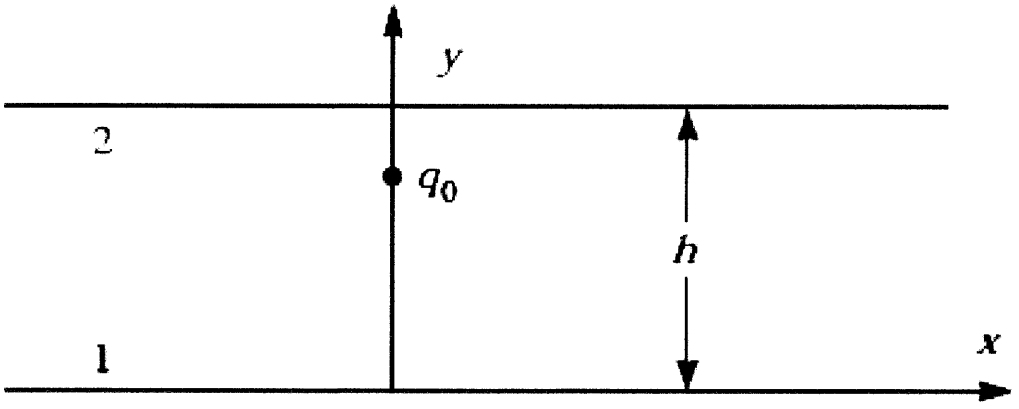

Figure 2-15: Figure 1.2 of Matheison's *Induced Charge Distributions in Proportional Detectors*. Reference for Eqs. 2.5 and 2.6.

that any source that is part way between two parallel plates, as in the set-up for this experiment, will not generate its full potential. While this distance can be calculated and the full potential extrapolated, there will still be difficult to measure effects from uneven collimation of the alpha beam.

However, by taking two measurements and switching the drift direction between them, these problems could be avoided. This works by adding an additional term to

equation 2.5 as follows:

$$P(y) = P_{12}\left(\frac{h-y}{h} + \frac{y}{h}\right) = P_{12} \tag{2.6}$$

This modification in experimental technique allows accurate collection of the full charge potential in the drift gas regardless of the source's location between the plates and collimation effects, as long as the alpha particles do not strike the plate's surface, thus imparting energy to the plate instead of to gas ionization. To avoid this, the source was placed a distance approximately halfway between the two plates and mounted parallel to them, as shown in Figure 2-16.

The second piece to consider is the movement of ions in the gas, as well as the electrons that provide the signal. These F ions drift through the gas at a rate around 100 times slower than the electrons, due to their mass. They also arrive at the collection instrumentation much more spread out, so they do not represent a problem in identifying the sharp rising peak of a wave of drifting electrons.

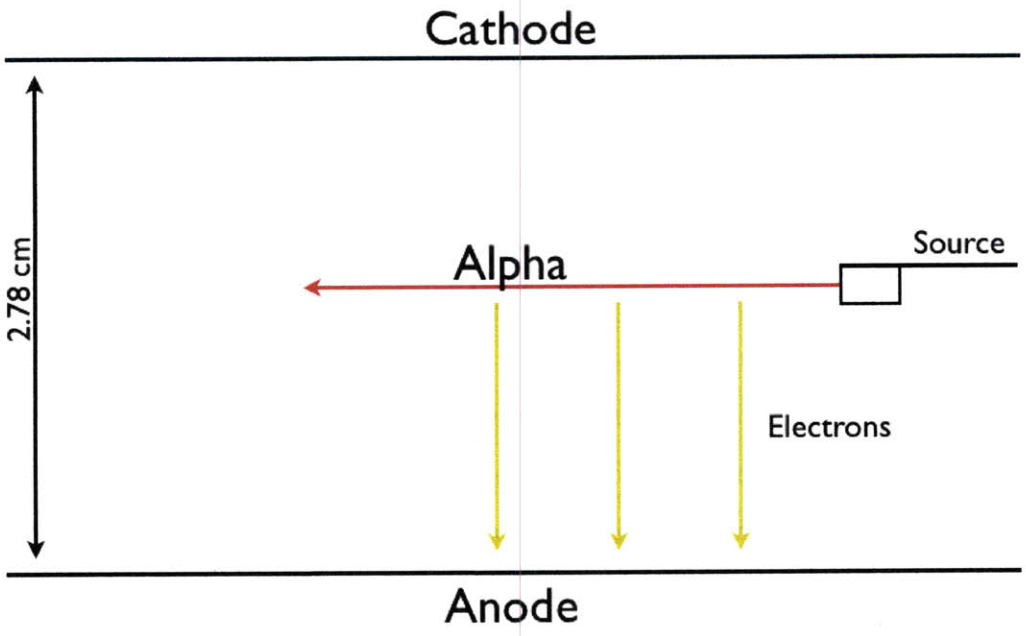

(a) Normal set-up

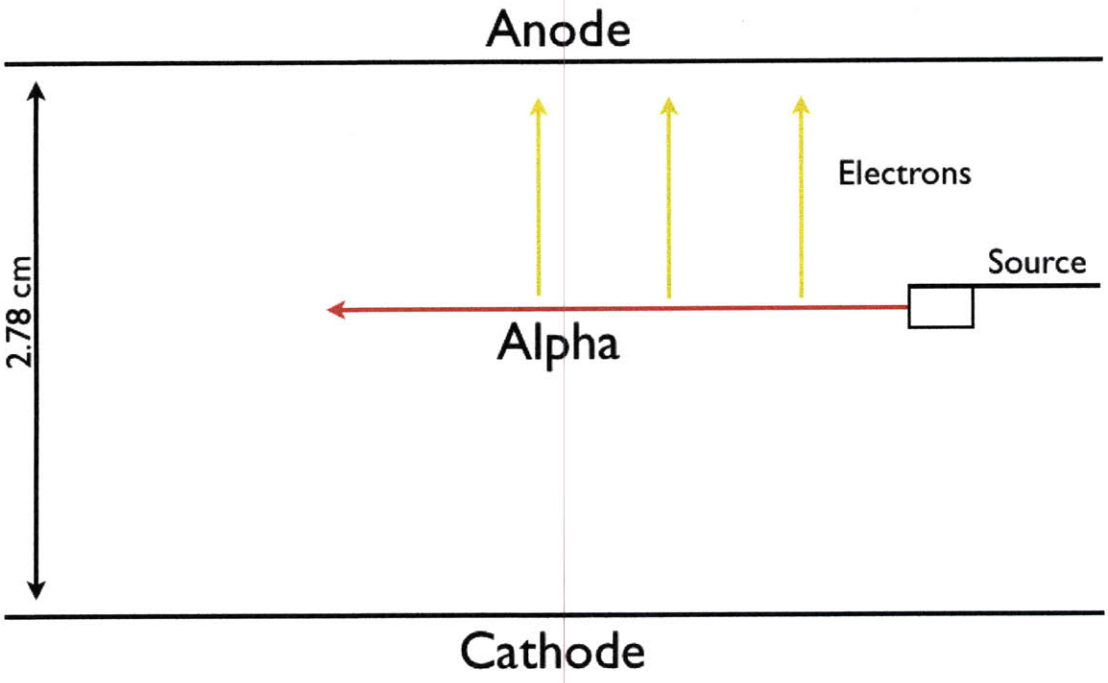

(b) Reversed set-up

Figure 2-16: Diagrams of the voltage switching set-up. In Figure 2-16(a) the electrons drift down as normal. In Figure 2-16(b) the anode and cathode are reversed, and the electrons traverse the distance up to the plate, covering the potential that was excluded in Figure 2-16(a).

Chapter 3

Results

This section elaborates on the procedure used to acquire the data. It describes the raw signal data, the binned runs, and the processed overlays of several runs, and what each of these data processing steps means in terms of W. Finally, it calculates the work function and discusses sources of error.

3.1 Raw Signal Data

The raw signal pulses received by the oscilloscope are very clear and well defined. Compared to the data collected in the old chamber set-up, the signal was approximately two times stronger, with about half as much signal noise (see Appendix A.1). The signal noise in the two plate set-up is on the order of 5 mV. This allowed for setting a low trigger to ensure that low amplitude pulses are not excluded from the data set. The trigger did occasionally have to be reset, as the noise amplitude grew with increasing voltage applied to the cathode. The peak noise encountered was at the maximum applied voltage of -2000 V, at which point sparking was more problematic than low-voltage noise (see Figure 3.1).

The preamplifier signal from an alpha track is shown in Figure 3-2. This is a typical and expected output given a negative pulse as was tested by a pulser. The rise time of the pulse is approximately 150 ns, followed by a 50 μs decay - much larger than the amplifier's rise time [12]. Thus, the amplifier will shape the pulse correctly

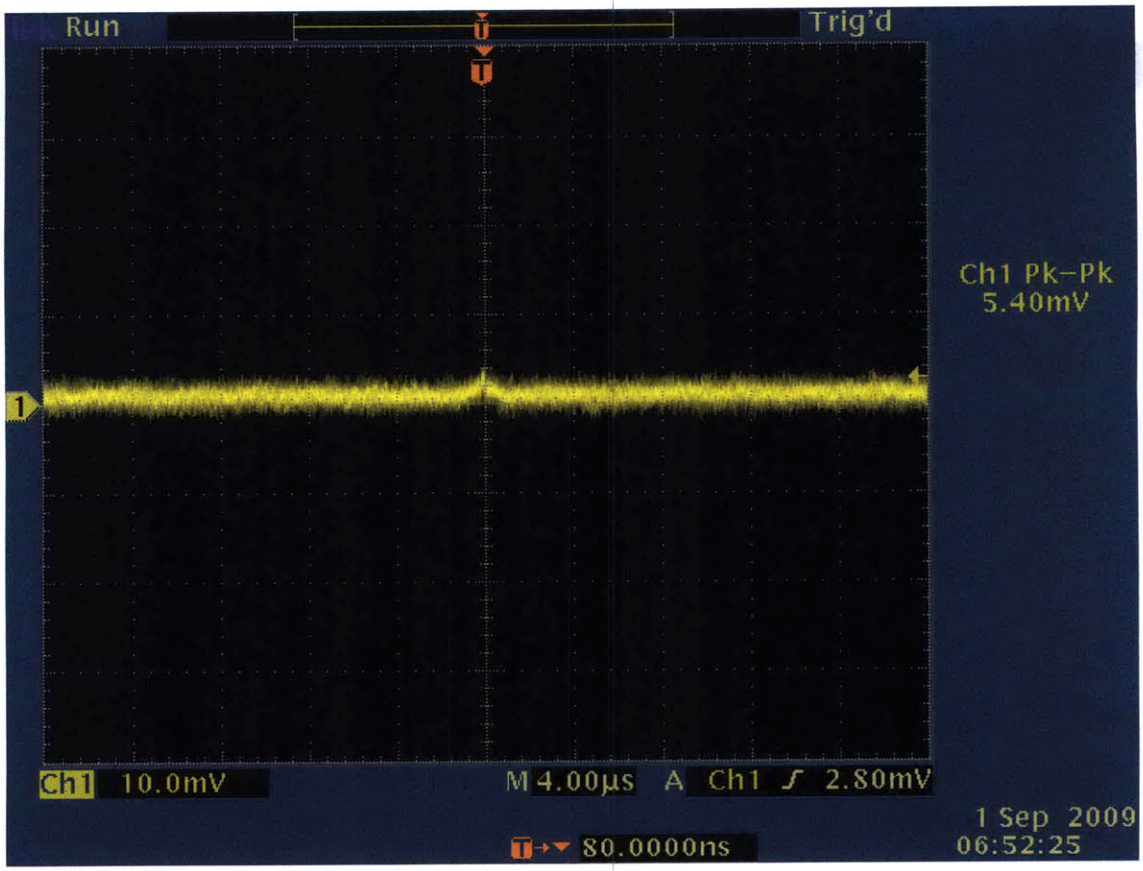

Figure 3-1: Noise profile of the dual-plate set-up through the entire electronics signal chain (including the amplifier). Signal noise is low and consistent on the order of 5 mV.

and without losing any signal charge in the process. The pre-amp pulse is well defined from the background noise, with an amplitude of 4 mV.

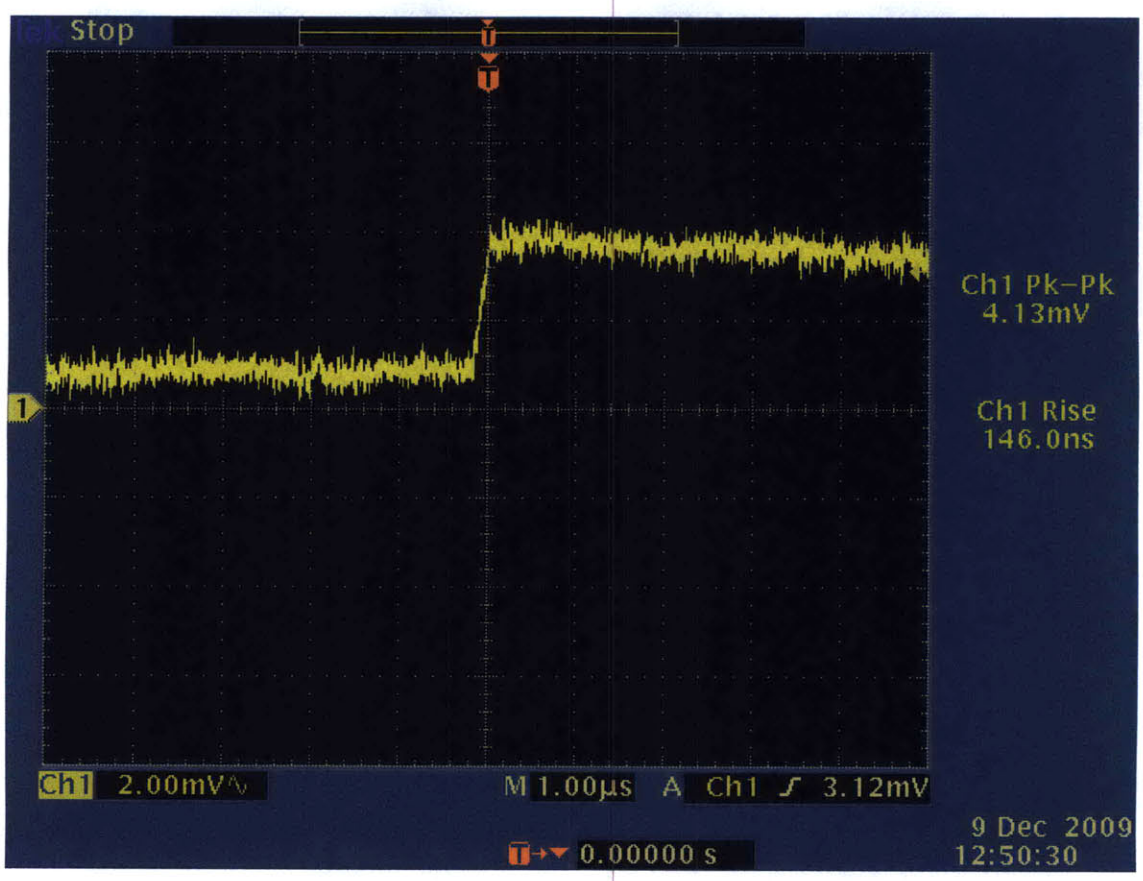

Figure 3-2: The preamplifier signal from an alpha event (no amplifier), during a test run. The rise time of 146 ns is much smaller than the amplifier's shaping time, so no charge is lost in the pulse shaping. The signal is well defined above the noise.

This pre-amp signal was then fed into the Canberra Amp/TSCA 2015A Amplifier. Examples of the amplifier signal are shown in Figure 3-3. The figure displays the signal clarity, with pulses on the order of 40 mV rising well above the 5 mV noise level at both 100 V and 800 V. At higher voltages (generally around 1500 V), sparking began to occur. This sparking had a different waveform than the alpha signal, as shown in Figure 3.1. These sparks first dip down before rising back up to the trigger. They tend to accumulate around certain peak to peak measurement values and can be cut by comparing the peak to peak versus maximum values. Peak to peak vs. maximum for an alpha pulse is approximately the same, while the peak to peak for a spark is roughly twice the size of the maximum. In this way, spark events can be cut from

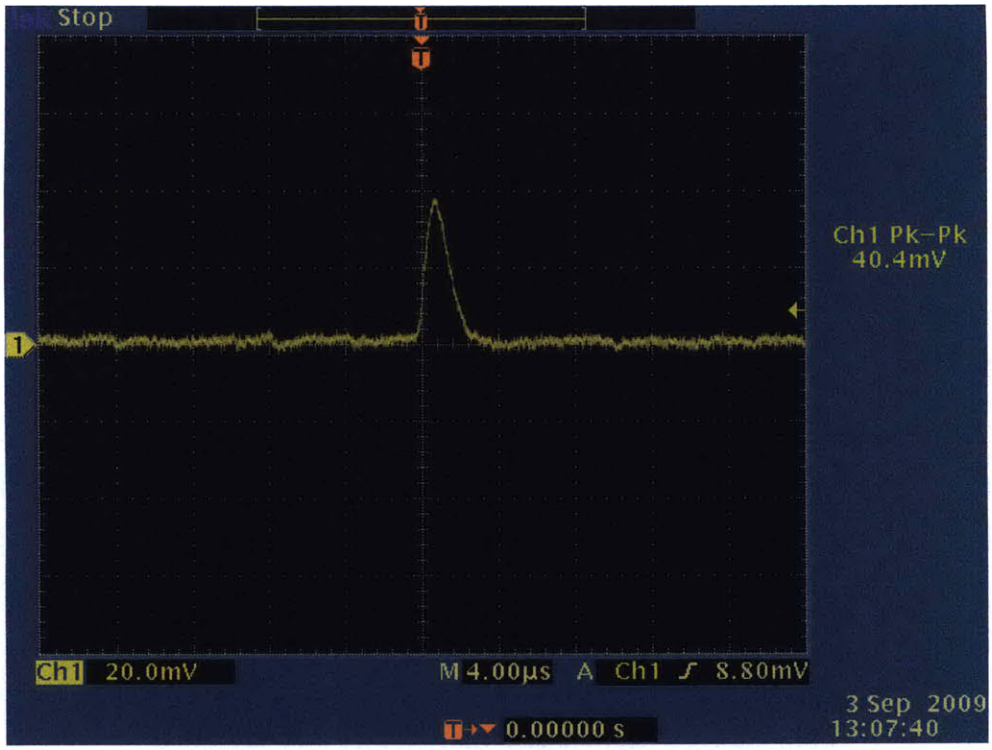

(a) 100 V

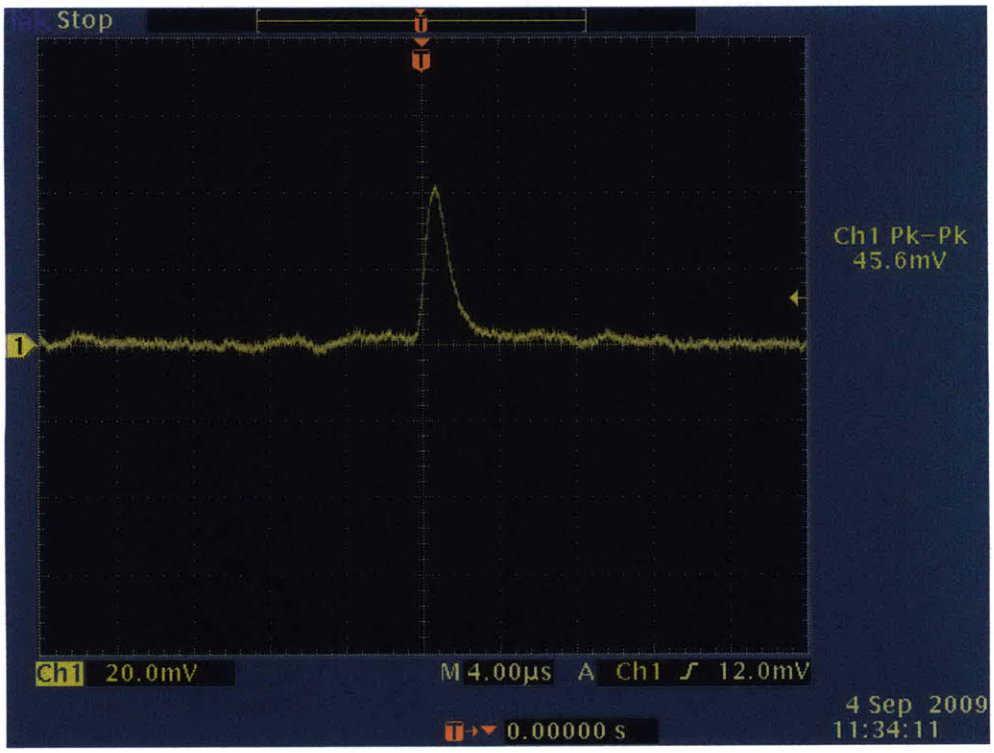

(b) 800 V

Figure 3-3: Examples of the amplifier signal at 150 torr CF_4. Figure 3-3(a) was taken at 100 V, and Figure 3-3(b) was taken at 800 V.

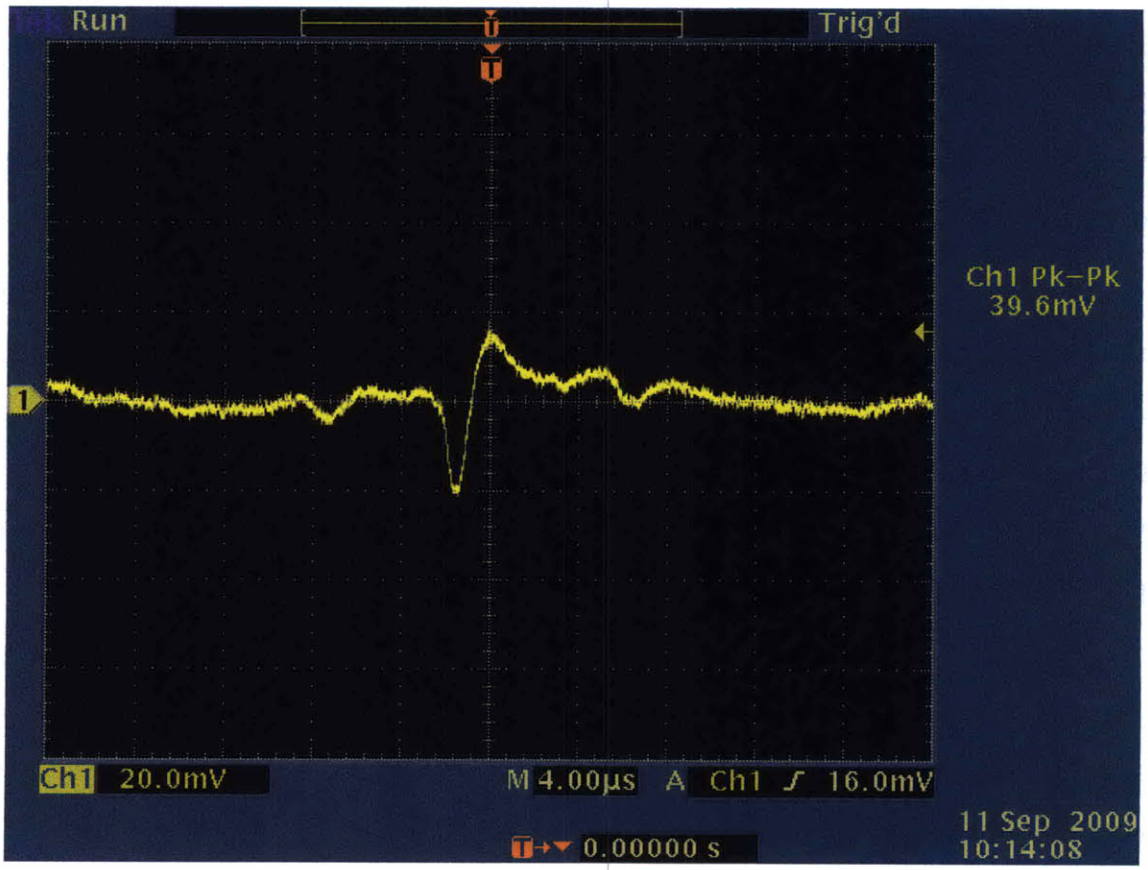

Figure 3-4: A spark at 1800 V and 150 torr CF_4. These signals differ significantly from the alpha signals and can be cut out by comparing peak-to-peak size to maxi size.

the data set.

3.2 Accumulated Runs at Constant Voltage

Each signal that triggers the oscilloscope is captured by the Root script. The waveform itself is not recorded, but variables such as peak to peak voltage and maximum voltage are transfered to a Root file for further analysis. For each voltage, a number of events between 100 and 500 was collected.

An example of a 500 sample run is shown in Figure 3-5(a). It was collected with the cathode set to -500 V with a chamber pressure of 150 torr. The data set has been fit with a gaussian in Root. The gaussian fit has a mean at 25.4 mV with an error on the mean of 0.2 mV. The spread of the gaussian, which represents some statistical variation in the number of electrons actually generated from any particular alpha particle, has a value of 3.7 mV.

As indicated in section 2.3, to arrive at the full value of the potential in a drift chamber, the anode and cathode must be reversed. The results of this reversal at +500 V are recorded in Figure 3-5(b). In this case, the fit has a mean at 31.8 mV with an error on the mean of 0.2 mV, and a spread (sigma) of 4.3 mV.

In order to arrive at the total voltage, the two mean values were added, as indicated in equation 2.6, for a total voltage of 57.3 mV. The errors on the mean, from the fit, were then added in quadrature. This procedure was then repeated at different values. The data for -1000 V at 150 torr is shown in Figures 3-6(a) and 3.2, and sums to 56.4 mV. The difference of the summed means between the different runs was then used to set the systematic error. The final value of the voltage, V, produced by the calibrated ^{241}Am alpha source was:

$$V = 56.8 \pm 0.3\ (stat) \pm 0.5\ (syst)\ mV \tag{3.1}$$

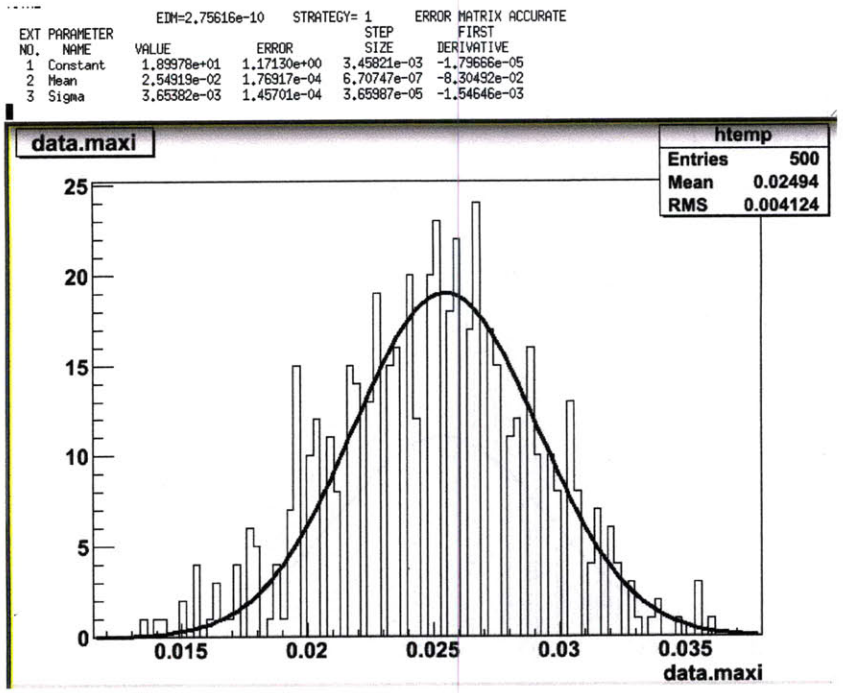

(a) -500 V. Mean: 25.4 mV Error: 0.2 mV Spread: 3.7 mV

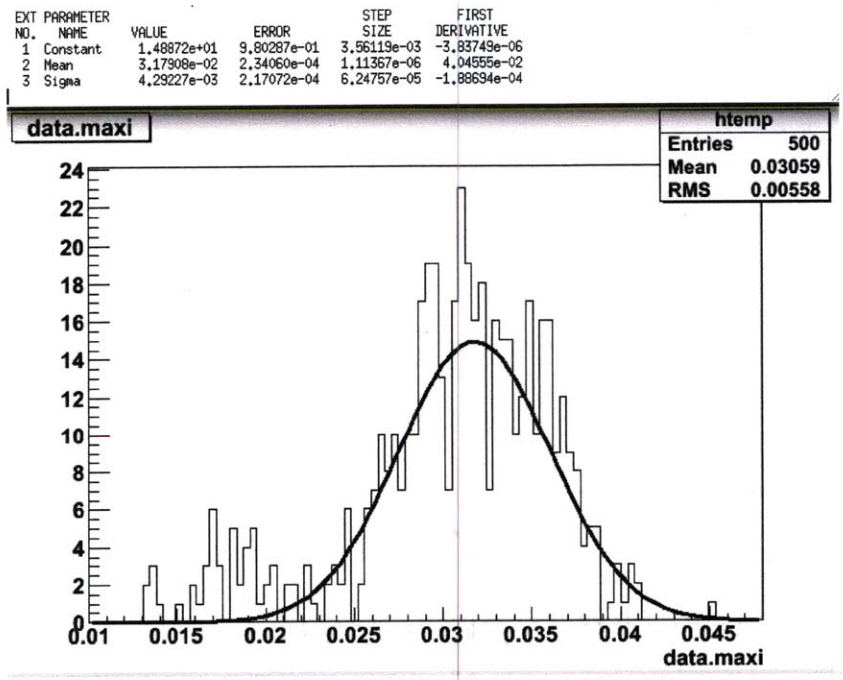

(b) +500 V. Mean: 31.8 mV Error: 0.2 mV Spread: 4.3 mV

Figure 3-5: Accumulated runs at ±500 volts. Each figure represents 500 data points at 150 torr CF_4. Fit data is shown above each run and summarized in the individual captions. The summed means is $57.3 \pm 0.4\ mV$ for $\pm 500\ V$ (Figure 3-5(a) and Figure 3-5(b)).

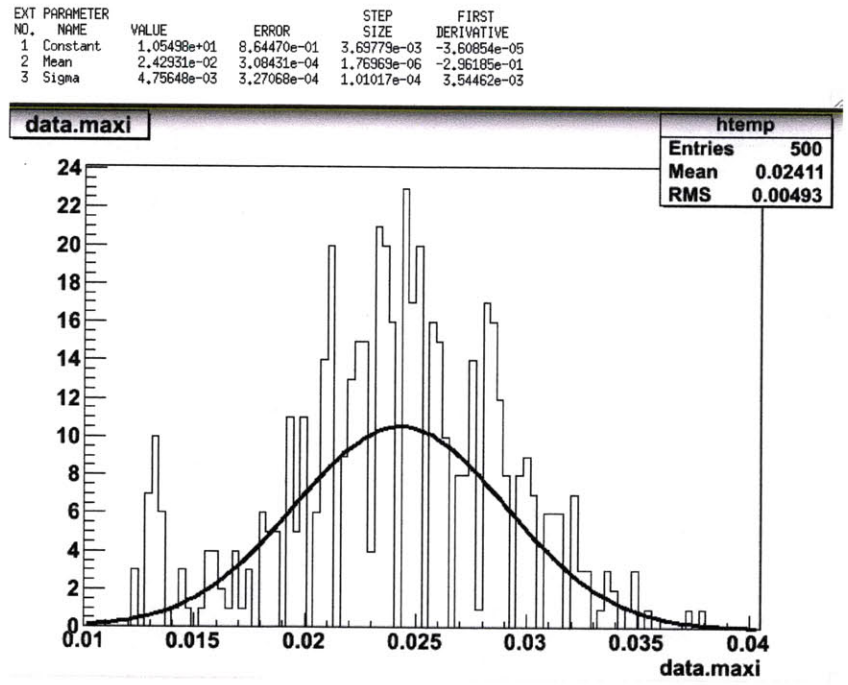

(a) -1000 V. Mean: 24.3 mV Error: 0.3 mV Spread: 4.8 mV

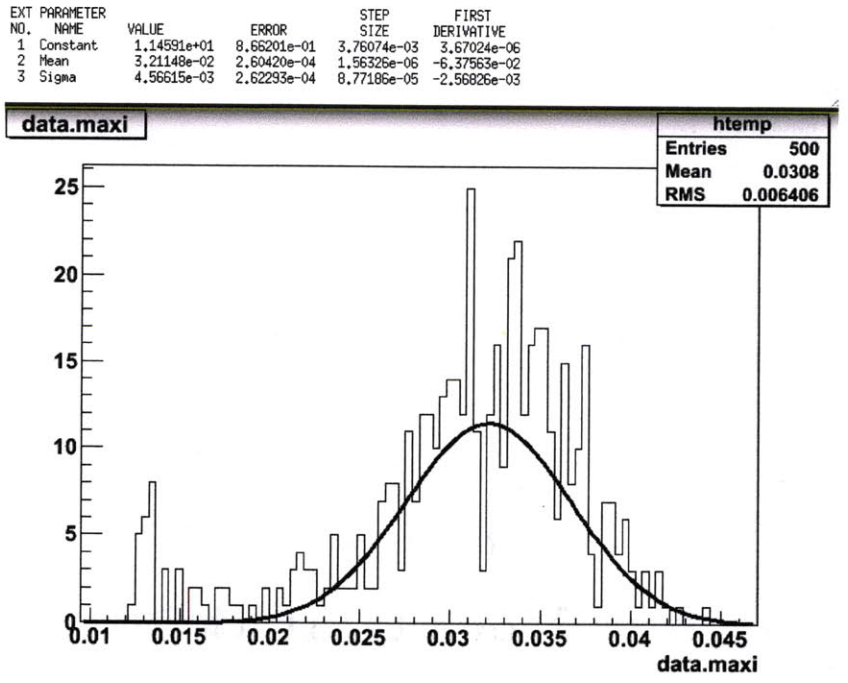

(b) +1000 V. Mean: 32.1 mV Error: 0.3 mV Spread: 4.6 mV

Figure 3-6: Accumulated runs at ±1000 volts. Each figure represents 500 data points at 150 torr CF_4. Fit data is shown above each run and summarized in the individual captions. The summed mean is $56.4 \pm 0.4\ mV$ for $\pm 1000\ V$ (Figure 3-6(a) and Figure 3.2).

3.3 Pressure Overlays of Run Profiles

In addition to the double measurements mentioned above in section 3.2 in which the anode and cathode were switched to provide the full potential voltage, there were a number of measurements made with a constant anode/cathode configuration. These were done to test stability of the result under different reduced drift fields. Additionally, these plots were made at multiple pressures to ensure that the value for V that was recorded was independent of pressure. If the measurement is indeed independent of pressure, then the plots should overlay each other nicely.

Figure 3-7 shows the results of these measurements. Each line represents a set of experiments done at a constant pressure: 75, 150, and 300 torr. Except for the initial measurements taken at around 20 V, all the points are on a flat line within statistical variations. This low voltage dip comes from the electric field being too low to drift all the electrons to the anode for collection. The flatness of the line signifies the plateau that gives the proper voltage to use in the work function equation, equation (1.9). This works as a check that the double measurements in which anode and cathode were reversed could be averaged to find a mean value, and ensures that the points chosen were not coincidentally located on similarly sized features.

No electron attachment or amplification region is seen in Figure 3-7 because the reduced electric field is too small [13].

Figure 3-7 also clearly indicates the independence of the measurement voltage peak-height from pressure. Each line of measurements at constant pressure lies nicely on top of the other lines within their standard deviation. Each set of measurements was run from about 20 V up to 2000 V, with the differences in length stemming from their different pressures. Finally, it is worth noting that the error on the 75 torr line is larger primarily because there was less data taken per run. This line of data was taken as a pressure check on the others, and so only 100 measurements were taken per run, as opposed to at least 200 measurements in the other pressure lines. This led to a somewhat less defined gaussian shape, and a flatter fit, which results in a larger sigma.

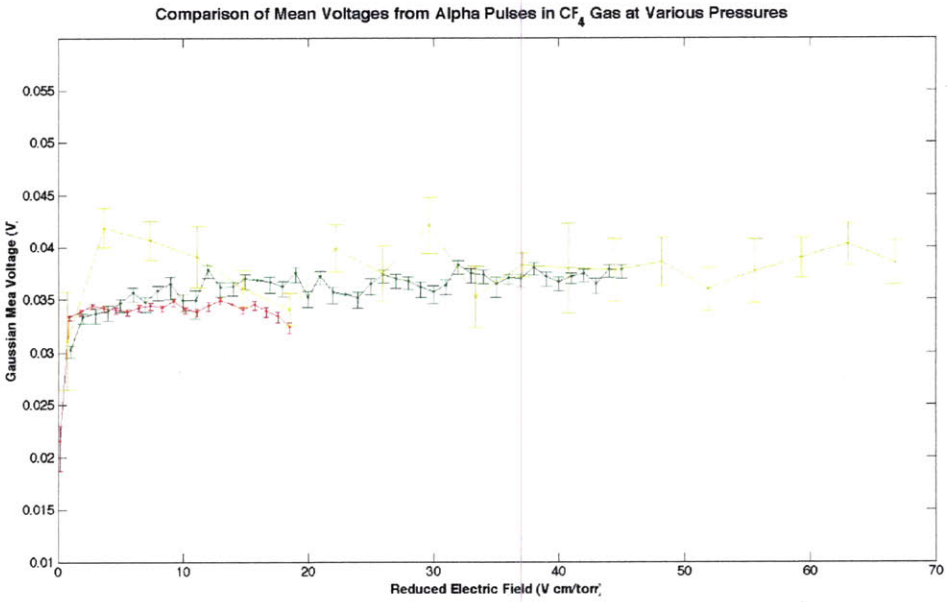

Figure 3-7: This plot shows the means of the accumulated runs plotted on top of each other. Each color represents a set of trials at a constant pressure. The runs have been adjusted from voltage to reduced electric field, so that they may be compared. The runs lie together very well, suggesting proper localization of the 'voltage plateau'. Each of these profiles were accumulated using single polarizations (ie. no cathode switching). As such, they are useful for identifying features, but do not give the actual location of the plateau.

3.4 Calculation of the Work Function

Bringing together equations (2.3), (2.4), and (3.1) and changing units, we have:

$$g = [2.80 \pm 0.003\ (stat) \pm 0.01\ (syst)] \cdot 10^{-12}\ V/C \tag{3.2}$$

$$Q_{e^-} = 1.602 \cdot 10^{-19} C \tag{3.3}$$

$$V = [56.8 \pm 0.3\ (stat) \pm 0.5\ (syst)] \cdot 10^{-3}\ V \tag{3.4}$$

$$E_\alpha = [4.282 \pm 0.005\ (stat) \pm 0.01\ (syst)] \cdot 10^{6}\ eV \tag{3.5}$$

Plugging these all into equation (1.9) gives:

$$\mathbf{W_{CF_4} = 33.8 \pm 0.2\ (stat) \pm 0.3\ (syst)\ eV} \tag{3.6}$$

3.5 Systematics

This section summarizes the sources of systematic error throughout the experiment, as well as comments on how this error was reduced or eliminated.

The first potential source of error was background noise contaminating the signal. This noise was reduced by shielding sensitive equipment, keeping cable lengths as short as possible (particularly between the detector and the preamplifier), connecting power sources in a way that reduced or eliminated ground currents, and powering down all unnecessary power sources, such as that of the vacuum pump once proper pressure had been achieved. A picture of the noise signal can be found in Figure 3-1, under amplification from both the preamplifier and amplifier. As the amplitude of the noise is about 1/10th the amplitude of the alpha signal, this noise would have a very small effect on spreading the peak of the signals collected. Since this error shows up in the spread, and not the mean or the error on the mean, and because of the small effect this spreading would have, this source of error was neglected for the final error calculations.

A further source of systematic error possibly comes from non-linearity of the

preamplifier and the amplifier. Both pieces of electronics were found to be extremely linear to a range far beyond that used in the experiment, a range that was explored in greater detail in Figures 2-2 and 2-5. No correction was necessary to account for linearity, and the amount of error propagating through the error calculations was taken to be negligible.

While the electronics were found to be quite linear, there is a source of systematic error stemming from the offset from zero. The fit on the gain calibration, found in Section 2.1.2, particularly Figure 2-7, did not intersect the origin perfectly, instead passing 0.042 V above it. This error was taken as a percentage of the slope, 9.230, and propagated through to the gain number.

There is finally some systematic error introduced in processing the voltage data into one unified figure to be used in equation 1.9. When the means of both polarities at a constant voltage are added for several voltages, there is some variation in the summed voltage. The actual number used was the mean of these voltages, and the spread was taken as the systematic error. This resulted in a systematic error of 0.5 mV on the voltage figure.

All of these numbers were added in quadrature to find the final systematic error on the measurement, W, to be 0.3 eV.

Chapter 4

Crosscheck with P10

A great way to check the systematics of the experiment is to use the same procedure on a different test gas with well known properties. P10 was chosen as a gas because it is relatively fast, which is important due to the shaping time of the collection electronics, and because the work function of P10 is well known at $W = 26.6$ eV.

4.1 Background Noise

One difficulty in working with P10, however, is that it is sensitive to noise signals that CF_4 is not. Figure 4-1 displays the preamplifier signal under a pressure of 150 torr, with the cathode voltage set to -300 V. The alpha source is the same as that used for CF_4.

The noise signal in Figure 4-1 is periodic, with an amplitude of around 1 mV. This noise did not prevent good triggers, as the pulses from the preamplifier were on the order of 3 to 5 mV. It does cause some spreading of the peak, adding an additional layer of uncertainty to the final measurement of P10's work function. In addition, because of the presence of this noise, all the data was taken strait from the preamplifier and not through the spectroscopy amplifier. This allowed me to cut out portions of the data that did not exhibit a proper rise time (on the order of 500 ns, as shown in Figure 4-1).

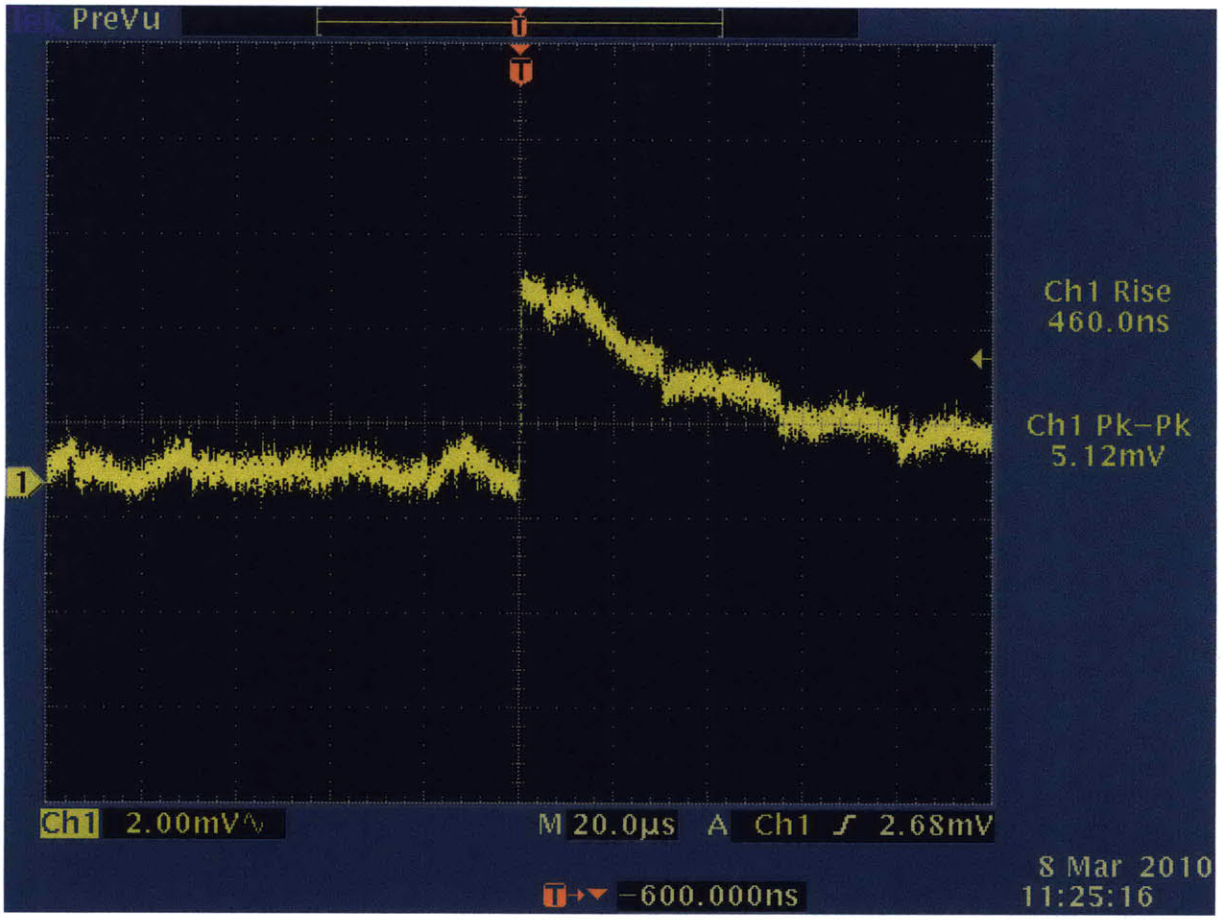

Figure 4-1: The preamplifier signal at 150 torr and -300V in P10. Notice the persistent noise signal at around 220 kHz, most likely caused by an unshielded computer clock or power source of undetermined origin.

4.2 Raw Data and Fitting

As before, the oscilloscope signals were collected via computer and compiled into histograms. I took several thousand signals to build a high-statistics histogram before the data was submitted to a gaussian fit in Figure 4-2.

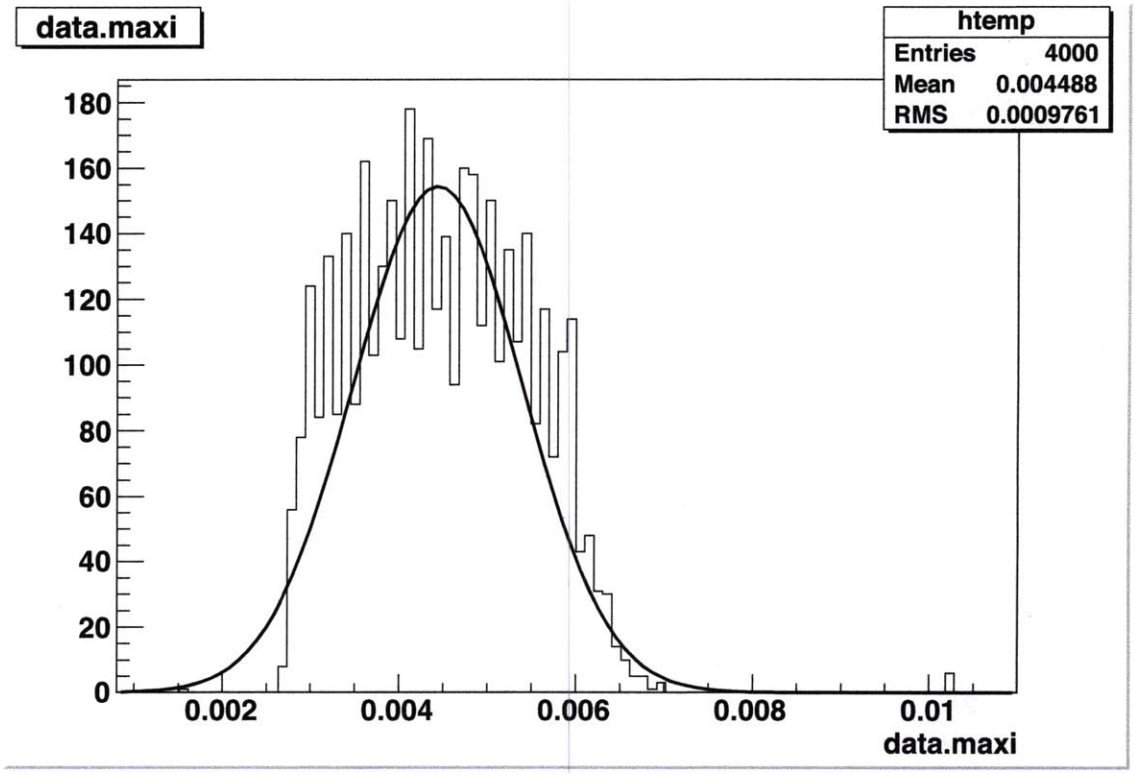

Figure 4-2: A collection of 4000 alpha signals, collected at 150 torr and -300 V. The shape is somewhat 'squarish' because of noise spreading and because the trigger was set to 2.68 mV to avoid large numbers of noise signals. The figure shows a gaussian fit of the data.

The data shows a somewhat squarish and lopsided shape because of noise spreading from the peak and because the trigger is set right on the leading edge, cutting out the left tail. It was set at this point (2.68 mV) to avoid capturing a large number of noise signals. However, this does shift the mean of the gaussian somewhat to the right, which will result in a somewhat lower estimation of W, according to equation

(1.9).

The mean was calculated to be 4.49 ± 0.02 mV, with a spread of around 1 mV.

The estimation of W requires a reversal in the chamber's polarity, as detailed in Section 2.3. This was done, with the same process being carried out as above, and is shown in Figure 4-3.

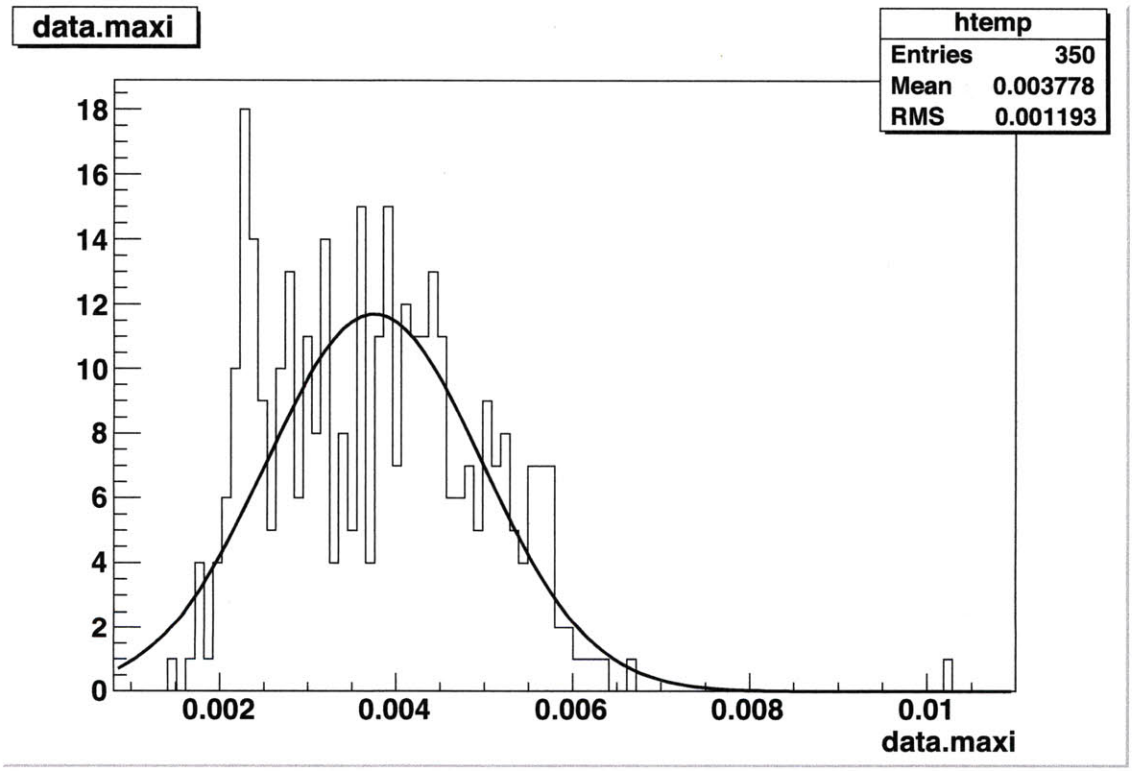

Figure 4-3: A collection of 1000 alpha signals, collected at 150 torr and +300 V (reversed anode/cathode). Notice the trigger was set somewhat lower on this run, at 2.08 mV, in an attempt to reduce how much the left hand tail was cut off. The figure shows a gaussian fit of the data.

The mean of the polarity reversed set of data is 3.75 ± 0.07 mV. The sigma is again around 1 mV.

Added together, the total voltage from the preamplifier set-up is 8.24 ± 0.07 mV.

4.3 Work Function of P10

Before numbers can be plugged into equation (1.9), however, a new calibration for g, the gain figure, must be completed. The set up is identical to the gain calibration of Section 2.1.2, with the exception of removing the amplifier from the signal chain. The form of equation 1.9 predicts that the gain will go down to compensate for the smaller signal size.

The gain calibration and linear fit for the preamplifier when connected to the detector is shown in Figure 4-4.

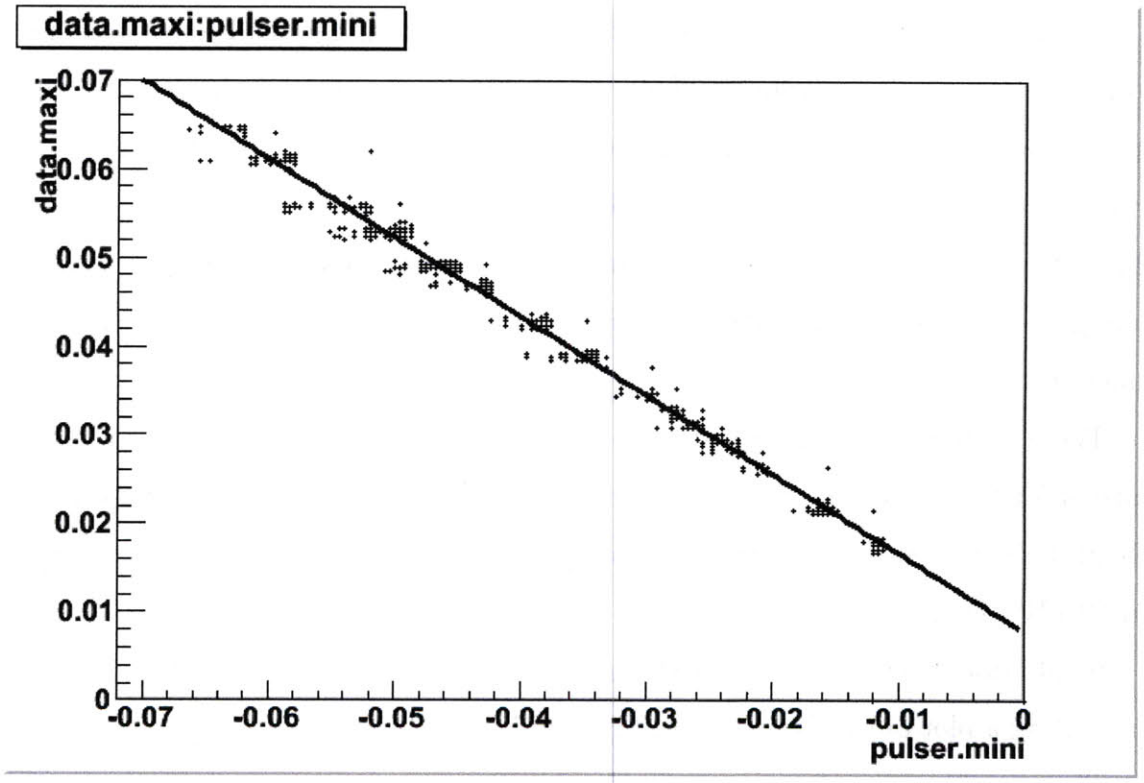

Figure 4-4: Preamplifier gain calibration. The plot shows preamp voltage against pulser input voltage, in volts. The fit has a slope of -0.887 and runs 0.008 V above the origin.

The slope of the fit is -0.887. The negative slope indicates proper reversal of the signal polarity from a negative pulser signal to a positive output signal. According to equation 2.2, the gain is then:

$$g_{preamp} = 0.269 \pm 0.002 \; V/pC \tag{4.1}$$

As the alpha source used was identical to that used for CF_4, a number can be returned from equation 1.9.

$$W_{P10} = 22.4 \pm 2.7\ (stat) \pm 3.0\ (syst)\ eV \tag{4.2}$$

4.4 P10 Systematics

The most immediate thing noticed in the P10 work function is that it is approximately one standard deviation lower than the known figure.

The non-negligable noise meant that the oscilloscope trigger had to be set higher to avoid capturing noise signals. This, in combination with the fact that the peak spreads down further past the trigger, led to a signal cut-off of around 2.5 mV. It is evident from Figure 4-2 that the peak should extend below this cut off. The effect of this is to shift the fit to the right, setting a higher mean voltage than is proper. As voltage appears in the denominator of equation (1.9), this artificially lowers the work function.

These factors result in an estimated shift in voltage of about 1 mV from the current sum. This error propagates through to result in a total systematic error of about 3 eV. In combination with the statistical error of 2.7 eV, there is a total error on P10 W of 4.1 eV.

In addition, because of time constraints, a minimal amount of P10 data was taken, preventing a plot of the form seen in Figure 3-7.

These problems are largely specific to the P10 measurement and are not factors that would affect the CF_4 measurement of W. The crosscheck with P10 shows the validity of the CF_4 measurement.

Even if the crosscheck on P10 is taken as evidence of a 20% inaccuracy in the CF_4 measurement, the work function would be grouped much closer to Reinking's assessment of W, suggesting a W on the order of 30 eV, not the 56 eV suggested by Sharma.

Chapter 5

Conclusions

This thesis has made an independent measurement of the work function of CF_4 and found it to be 33.8 $\pm$ 0.4 eV. In doing so, it settles the conflict established between the values of Sharma (56 eV) and Reinking et. all (34.3 eV). While the agreement between this thesis' findings and Reinking are not perfect, they do establish the work function for CF_4 at around 34 eV, important for particle drift detectors like the Dark Matter Time Projection Chamber, for which this study was undertaken. Due to the fact that Reinking et. all did not provide error on their number for W, the two results could not be combined with any certainty.

All three findings, as well as those listed in [6], are plotted in Figure 5-1. This figure shows the good agreement between most alpha and beta measurements for gases, as well as the large disparity between past measurements of CF_4. The red star is the marker for the measurement of this thesis, which is in solid agreement with the measurement of Reinking et. all.

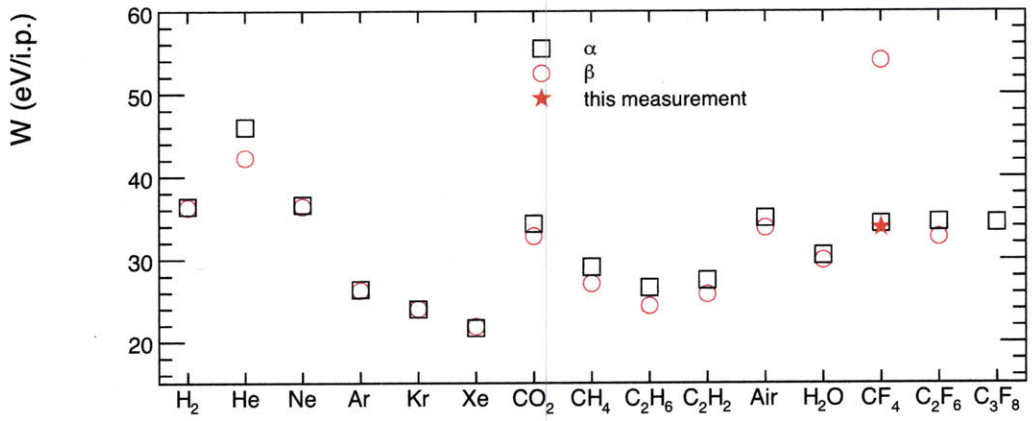

Figure 5-1: This figure compares the work functions of several different gasses and mixtures. The black squares are the work function from alpha particles, while the black circles are from beta particles. The measurement from this thesis is imposed in the proper place on CF_4, agreeing quite nicely with the measurement of Reinking et al.

Appendix A

Relations to DMTPC Experiment

A.0.1 Anode Signal from WIMP Interaction

There are a range of possible voltage signals from a dark matter interaction in the DMTPC detector. This range of energies is derived from Lewin [9]:

$$\frac{dN}{dE} = e^{-E_R \ / \ (E_0 \cdot r)} \tag{A.1}$$

N is the event rate per unit mass, and E is the energy, which makes equation A.1 a differential energy spectrum. This is expected to be smoothly decreasing, and this is evident in the form of the right side of the equation, where E_R is the recoil energy, E_0 is the most probable energy of dark matter:

$$E_0 = \frac{1}{2} M_D \cdot v^2 \tag{A.2}$$

M_D is the mass of dark matter, which was taken to be 100 GeV, and v is the rotational speed of the galaxy, 220 km/s. The r of equation A.1 represents a kinetic factor:

$$r = \frac{4 M_D \cdot M_T}{(M_D + M_T)^2} \tag{A.3}$$

where M_T is the mass of the target nucleus, which for DMTPC is Flourine, 19 GeV.

Relating this equation to W comes through the following:

$$V = E_R \cdot \frac{Q_{quench}}{W} \cdot Q_{e^-} \cdot \frac{G_{charge}}{g} \tag{A.4}$$

The quenching factor, Q_{quench}, is set to 1, because approximately all recoil energy should be dissipated in the drift gas. The detector gains are taken into consideration with G_{charge} the gas gain, which was set to 10^4 for this calculation, and the electronics gain, g, taken to be 0.15 V/pC. Finally, Q_{e^-} is the charge of the electron.

Solving for E_R gives:

$$E_R = V \cdot \frac{W \cdot g}{Q_{e^-} \cdot G_{charge}} \tag{A.5}$$

Finally, plugging equation A.5 in to equation A.2 results in:

$$\frac{dN}{dV} = e^{-\left[\frac{(V \cdot W \cdot g)}{(Q_{e^-} \cdot G_{charge}) \cdot (E_0 \cdot r)}\right]} \tag{A.6}$$

Equation A.6 was then plotted in Figure A-1 for both Sharma and Reinking's declared values of W.

A.1 Mesh Effects

It is difficult to measure the work function in the DMTPC chamber because of the chamber set-up. A copper mesh is spread about 2 mm above the surface of the anode. During normal operation this copper mesh helps create the region of high electric field inside the chamber that creates an electron cascade. The mesh is set to ground and a positive bias is applied to the anode (the anode is set to ground in this thesis).

Mesh effects are not an issue in the DMTPC set-up because of the high voltages required to cause an electron cascade. At high voltages, the mesh is transparent to electrons. The intense electric field channels the electrons through the gaps in the mesh. However, the experiment in this thesis runs below this cascade threshold in order to accurately determine the number of electrons ionized by the radiation source, so a significant percentage of the electric field lines terminate on the mesh instead of

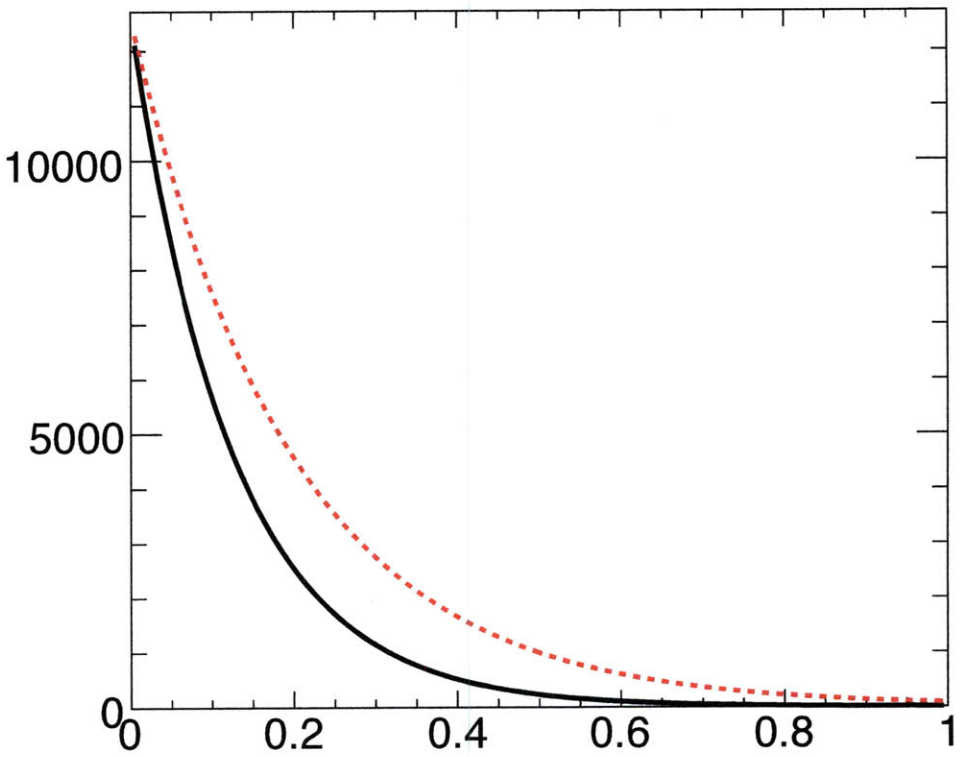

Figure A-1: The anode voltage response to dark matter scattering spectrum. The horizontal axis is in Volts, the vertical in arbitrary units $\frac{dN}{dV}$. The solid black line is the work function according to Sharma (54 eV), and the dashed red line is Reinking's assessment (34.3 eV).

passing through it. This causes the mesh to collect electrons and shunt them off to ground, reducing the number of electrons that pass through and are collected on the anode plate.

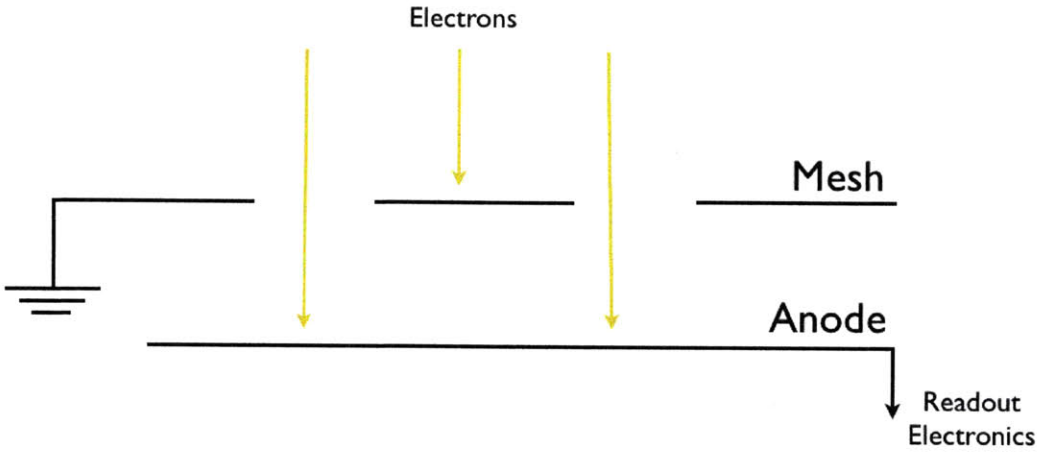

Figure A-2: Diagram of electron interaction with the mesh in small electric fields (ie. low voltage between the mesh and the anode). Instead of being channeled through the gaps in the mesh, some of the field lines terminate on the mesh, causing signal loss.

Bibliography

[1] F. Zwicky, Astrophys. J. **86**, 217 (1937).

[2] J. Hogan, Nature 242, 448 (2007), http://www2.lns.mit.edu/ LQS/Nature%20-%20dark%20matter.pdf

[3] R. J. Gaitskell, Ann. Rev. Nucl. Part. Sci. **54**, 315 (2004).

[4] D. N. Spergel, Phys. Rev. D **37**, 1353 (1988);

[5] J. F. Ziegler, J. P. Biersack, U. Littmark, Pergamon Press, New York (1985).

[6] W. Blum, L. Rolandi and W. Riegler, *Berlin, Germany: Springer (2008) 448 p*

[7] A. Sharma, 3, GSI-Darmstadt, Germany.

[8] G.F. Reinking, L.G. Christophorou, S.R. Hunter, J. Appl. Phys. 60 (2), **500** (15 July 1986).

[9] J. D. Lewin and P. F. Smith, Astropart. Phys. **6**, 87 (1996).

[10] http://www.canberra.com/pdf/Products/NIM_pdf/2006_SS.pdf

[11] http://www.ortec-online.com/electronics/pulse/419.pdf

[12] http://www.canberra.com/pdf/Products/NIM_pdf/C37618-2015B-SS.pdf

[13] T. Caldwell *et al.* [DMTPC ollaboration], arXiv:0905.2549 [physics.ins-det].